Theses and Dissertations

May 2021

Development of Novel Compound Controllers to Reduce Chattering of Sliding Mode Control

Mehran Rahmani
University of Wisconsin-Milwaukee

DEVELOPMENT OF NOVEL CONTROLLERS TO REDUCE CHATTERING OF

SLIDING MODE CONTROL

by

Mehran Rahmani

A Thesis Submitted in

Partial Fulfillment of the

Requirements for the Degree of

Master of Science

in Engineering

at

The University of Wisconsin-Milwaukee

May 2021

ABSTRACT

DEVELOPMENT OF NOVEL COMPOUND CONTROLLERS TO REDUCE
CHATTERING OF SLIDING MODE CONTROL

by

Mehran Rahmani

The University of Wisconsin-Milwaukee, 2021
Under the Supervision Professor Mohammad H. Rahman

The robotics and dynamic systems constantly encountered with disturbances such as micro electro mechanical systems (MEMS) gyroscope under disturbances result in mechanical coupling terms between two axes, friction forces in exoskeleton robot joints, and unmodelled dynamics of robot manipulator. Sliding mode control (SMC) is a robust controller. The main drawback of the sliding mode controller is that it produces high-frequency control signals, which leads to chattering. The research objective is to reduce chattering, improve robustness, and increase trajectory tracking of SMC. In this research, we developed controllers for three different dynamic systems: (i) MEMS, (ii) an Exoskeleton type robot, and (iii) a 2 DOF robot manipulator. We proposed three sliding mode control methods such as robust sliding mode control (RSMC), new sliding mode control (NSMC), and fractional sliding mode control (FSMC). These controllers were applied on MEMS gyroscope, Exoskeleton robot, and robot manipulator. The performance of the three proposed sliding mode controllers was compared with conventional sliding mode control (CSMC). The simulation results verified that FSMC exhibits better performance in chattering reduction, faster convergence, finite-time convergence, robustness, and trajectory tracking compared to RSMC, CSMC, and NSFC. Also, the tracking performance of

NSMC was compared with CSMC experimentally, which demonstrated better performance of the NSMC controller.

Keywords: Chattering, Exoskeleton robot, MEMS, Robot manipulator, Sliding mode control, Trajectory Tracking.

Dedication

To

My Beloved Family

TABLE OF CONTENTS

LIST OF FIGURES

LIST OF TABLES

LIST OF ACRONYMS

DoF   -   Degree of Freedom

FSMC   -   Fractional Sliding Mode Control

MEMS   -   Micro Electro Mechanical Systems

NSMC   -   New Sliding Mode Control

RSMC   -   Robust Sliding Mode Control

SMC   -   Sliding Mode Control

SMS   -   Sliding Mode Surface

ACKNOWLEDGEMENTS

Chapter 1

Introduction

In control theory, robust control is a method for controller design that is directly related to modeling uncertainty, and unknown disturbances. The goal of the robust control method is to design a controller to obtain robust performance and/or stability in the presence of bounded modeling errors [1, 2]. Sliding mode control (SMC) is a nonlinear control method used in control systems to change the behavior of a nonlinear dynamic system by applying a discontinuous control signal that causes the system to "slide" along a sliding surface. The state-feedback control law is not a continuous function of time.

The main problem of the sliding mode control is that it creates chattering, which is responsible for damaging the structure of mechanical systems [3]. Scholars are designed different control approaches to reduce the chattering of SMC. For example, Kachroo and Tomizuka [4] used a boundary layer around the switching surface to eliminate chattering in the SMC. The novelty of designing sliding mode control depends on how to select sliding mode surface.

In this research, three controllers that include robust sliding mode control (RSMC), new sliding mode control (NSMC), and fractional sliding mode control (FSMC) based on sliding mode control are proposed. These control methods are applied on a MEMS gyroscope, an exoskeleton robot, and a 2DoFs robot manipulator. The simulation results demonstrated that FSMC shows better performance in chattering reduction, faster convergence, robustness, and trajectory tracking compared to three other controllers, CSMC, RSMC, and NSMC. The main contributions of this research are as follows:

- A novel FSMC was proposed to improve tracking performance

- Experimental verification of the proposed NSMC on a 2DoFs robot manipulator showing better trajectory tracking performance compared to CSMC.

Chapter 2

Overview

2.1 Literature Review

In the literature review section, applications of different control methods on MEMS gyroscope, Exoskeleton robot, and robot manipulator are discussed.

2.1.1 Control of MEMS gyroscope

MEMS gyroscope devices, also referred to as angular rate sensors are widely used in control engineering to measure angular velocity without any fixed point of reference. The advantage of MEMS gyroscope is their small size, which makes them suitable for various applications, such as automotive and biomedical applications [5, 6]. MEMS gyroscope needs to be suitably controlled to perform its defined task, such as measuring angular velocity. Sliding mode control (SMC) is a conventional control system that has been used in various industrial MEMS applications [7-9]. Batur et al. [10] proposed an adaptive feedback controller using SMC to guarantee the stability of the MEMS gyroscope device. Fei and Yuan [11] proposed a dynamic SMC approach with a novel switching function for the state tracking of MEMS gyroscope. Simulation results verified that the proposed control method can improve the dynamic performance of the MEMS gyroscope.

The chattering phenomenon [12], which is caused by the unmodelled dynamics system (the phenomenon that is affected by the controller and external perturbation that are not observable by the model), is the main drawback of the SMC. Chattering is a quick, sometimes noisy vibration with a fixed frequency and amplitude. Generally, the chattering phenomenon can be eliminated by using a compound system. Chu and Fei [13] proposed an adaptive global SMC using a Radial Basis Function (RBF) neural network for the reduction of chattering and tracking of the MEMS

gyroscope. The proposed control method has suitable tracking performance, but high chattering in the control input is the main problem. Ren et al. [14] proposed an adaptive fuzzy finite time SMC on MEMS gyroscope to consider uncertainty and external disturbance. The stability of the proposed control system was verified by Lyapunov's theory. Wang and Fei [15] proposed a multi-input multi-output Takagi-Sugeno fuzzy model designed to improve tracking performance. The proposed controller improved the tracking performance, but it has high control inputs. Xin and Fei [16] proposed an adaptive backstepping sliding mode control method to control the x-y movements of the MEMS gyroscope. An adaptive backstepping controller was designed and incorporated with the SMC to estimate systems uncertainties. By designing (Xin and Fei [16]) the adaptive backstepping sliding mode controller, the chattering phenomenon was considerably eliminated. Fei et al. [17] proposed an adaptive nonsingular terminal sliding mode tracking control method based on the backstepping approach for MEMS gyroscope vibratory control. The proposed control method guaranteed the asymptotical stability of the closed-loop system. Ghanbari and Moghanni-Bavil-Olyaei [18] proposed a novel terminal sliding mode controller to control the MEMS z-axis gyroscope. However, using (Ghanbari and Moghanni-Bavil-Olyaei) an adaptive fuzzy terminal sliding mode controller, the chattering phenomenon was significantly reduced.

Several recent publications focused on the application of neural networks and fuzzy control to improve SMC performance [19]. Pour Asad et al. [20] proposed a new fuzzy SMC to control a MEMS gyroscope. A supervisory compensator was applied to eliminate the effect of the estimation error. Simulation results demonstrated that the type-2 fuzzy system performs better than the adaptive neuro-fuzzy SMC inference system (ANFIS). Chu et al. [21] proposed a global proportional integral derivative (PID) SMC based on an adaptive radial basis function neural network. A neural network was implemented to ensure stability and robustness in the presence of

a lumped uncertainty for a MEMS gyroscope system. Moreover, dynamic global PID sliding mode control and adaptive laws guarantee the asymptotic stability of the close-loop system.

Rahmani [22] suggested a novel hybrid fractional-order terminal sliding mode control and proportional-integral-derivative (PID) control to control a MEMS gyroscope. SMC is a robust control, and PID controller has high tracking performance. Therefore, both controllers use each other advantages. The differentiation and integration order of the operation can be defined as a real or complex number. The chattering problem in the fractional integral terminal sliding mode control was eliminated using a proportional-derivative (PD) controller. As the studies above have indicated, the chattering phenomenon in the SMC can be eliminated by choosing an appropriate control method. However, an optimal way of implementing the control method remains to be investigated.

2.1.2 Control of Exoskeleton Type Robots

An exoskeleton upper limb robot is one type of rehabilitation human-robot interaction, which has been widely studied by researchers all around the world. Sliding mode control has been widely used in robotics systems due to its high tracking performance and robustness against external disturbances [23-27]. Zhu et al. [28] proposed a new linear integral sliding mode control to enhance the tracking performance. Then, they applied a radial basis function (RBF) neural network to eliminate the chattering phenomenon created by the integral sliding mode controller. The proposed RBF neural network reduced chattering created by the integral sliding mode control. Long et al. [29] proposed a compound position control method, which combines a sliding mode control with a cerebellar model articulation controller neural network. To improve performance of sliding mode control, a genetic algorithm was applied to determine the optimal sliding surface and sliding control law. The simulation results demonstrated the effectiveness of the proposed control

that improved the trajectory tracking scheme on an exoskeleton robot. Wang et al. [30] proposed a sliding mode control of the electro-hydraulic servo system to track the desired trajectory tracking. It was observed that the electro-hydraulic servo system of the exoskeleton robot improved uncertainties and load disturbance by combining the sliding mode controller and RBF neural network. A control scheme tuned with a genetic algorithm applied for shoulder rehabilitation robot control improves tracking performance [31]. Mushage et al. [32] proposed a compound high-gain state observer and a fuzzy neural network for state vector and nonlinear dynamic estimation.

The proposed control method was applied on a 5-DOFs upper limb exoskeleton robot, which can track the desired trajectory appropriately. However, the main limitation of the fuzzy control method is to select/choose fuzzy rules, which need to be selected appropriately for an exoskeleton robot. The main drawback of the proposed control method is the high control input. Ahmed et al. [33] proposed a fractional-order nonsingular fast terminal sliding mode control for the lower-limb robotic exoskeleton in the existence of external disturbances and uncertainties [34]. The main advantage of the proposed control method is that it can control the exoskeleton robot without relying on the accurate dynamic model of that robot. However, the proposed control method created high control input. Achili et al. [35] proposed an adaptive observer-based controller both on a Multi-layer perceptron neural network (MLPNN) and a sliding mode method for control of a wearable robot. The MLPNN, selected for its features of estimation, has been applied to identify the unknown dynamic. The proposed research validated the control method in terms of trajectory tracking both in simulation and experimentation. Han et al. [36] proposed model-free adaptive nonsingular fast terminal sliding mode control, which includes three parts: the intelligent PI controller, time delay estimation, and adaptive sliding compensator. By applying the proposed control method, tracking error converged to zero in finite time [37]. Mefoued [38] designed an

6

adaptive MLPNN which does not require the dynamic model of the system. Rahman et al. [39] applied a sliding mode control method on a 7-DOF exoskeleton robot. Experimental results verified that SMC effectively maneuvers an exoskeleton robot to track the desired trajectory. Later on, Brahim et al. [40] proposed a new control scheme based on human upper-limb inverse kinematics to improve the trajectory tracking performance in Cartesian space. All the works mentioned above, however, lack the essential control features such as robustness or convergence of trajectory tracking error to zero in finite time. Therefore, by observing these problems, we decided to design a novel control method that includes all the mentioned advantages.

2.1.3   Control of robot manipulator

SMC is a powerful controller for robustness and trajectory tracking [41-46]. Xiong et al. [47] introduced distributed SMC under the quantization process. To use digital communication, a quantizer is produced on the sensor system [48]. For the sensor system, an integral SMS is used on the basis of the filtered signal. Simulation results verified the improved trajectory tracking performance of the proposed controller. Herrera et al. [49] used the Alpeter method and SMC to produce a dynamic SMC. A comparison of the suggested method and SMC illustrated the advantages of the proposed control. The proposed controller reduced chattering. Yu et al. [50] proposed a new control scheme for the piezoelectric actuator to obtain suitable tracking performance. A particle swarm algorithm was used for the identification of nonlinear model parameters. The proposed structure, SMC, and feedforward methods are applied using the Bouc-Wen inverse algorithm to improve the position tracking performance. Wang et al. [51] introduced incremental nonsingular SMC for nonlinear systems regarding sudden actuator fault, external perturbations, and model uncertainties. This scheme does not include singularity [52] because it is free from any negative fractional order. The simulation result illustrates that the proposed scheme

is robust against actuator faults compared to Li et al. [53] proposed a novel asynchronous dynamic output feedback SMC method for a singular markovian jump system and considered the problem of asynchronous output feedback SMC design.

Zheng et al. [54] introduced a fuzzy SMC approach to control the robot with perturbations. The complex dynamic model of the robot has been considered by using perturbations. New fuzzy SMC is proposed according to SMC and fuzzy control combination. A deep learning method is applied to achieve a precise dynamic model experimentally. Deep learning estimates the dynamic model perfectly. Experimental results on KUKA robot verified the performance of the intelligent fuzzy SMC approach in terms of tracking performance. Jing et al. [55] introduced a novel adaptive SMC to perturbation rejection method and applied it to the robotic manipulator. Some modifications based on tracking error were implemented by applying certain functions to guarantee the steady-state and the transient performance of robotic arms. First, a nonsingular SMS is implemented by applying the modified error. Then, to stabilize the system, a terminal SMC was used. Next, a new sliding mode observer was applied to suppress external disturbances and compensate for the uncertainties. An adaptive algorithm generated from equivalent control was proposed for considering lumped disturbance [55]. The adaptive SMC was designed by Jing et al. in a combination of nonsingular terminal SMC, adaptive algorithm, and sliding mode disturbance observer. The performance of the designed controller is verified by different simulations. Ferrara et al. [56] introduced a controller for an industrial robot manipulator by using a switching method. Two cases are proposed in this controller: inverse dynamic and decentralized methods. The first one is suitable for improving the velocity and acceleration performance, and the second one is convenient for suitable compensate external perturbations. Therefore, the integral SMC is applied to approximate the unmodeled dynamic and compensate matched perturbations by correction of

error value. Yi and Zhai [57] considered an adaptive second-order fast nonsingular terminal sliding mode control when inertia uncertainties and external perturbations are applied to a robotic manipulator.

Chattering has been eliminated by using adaptive sliding mode control. A second-order fast nonsingular terminal SMC is applied to obtain desirable tracking and fast convergence and ensure robustness and system performance. It's not required to use the upper bound by applying the adaptive algorithm. Xia et al. [58], to control uncertain systems with time delay, proposed robust SMC. The robust reaching control algorithm is used for sliding mode surface based on the linear matrix. Zhang and Yan [59], to control piezoelectric system, proposed an adaptive observer integral SMC. An adaptive observer is designed to suppress the noises by using a Dahl estimation approach. To achieve chattering elimination, fast convergence, and robustness, the parameter of the SMC is adaptively tuned. Che et al. [60] considered a singularity problem with input nonlinearity by proposing observer-based adaptive integral SMC and passivity analysis. Linear matrix inequalities problems were solved by using passivity conditions [60]. Then, a singular disturbance observer is implemented to estimate the design of adaptive law.

Also, to obtain the controller parameters of integral SMC, a set of the matrix was used. Erenturk [61] used two control systems, SMC and an optimized PID controller, to control a two-mass structure. A grey estimator is applied to optimize the proposed controller. Experimental results suitably verified the applied controller performance in terms of trajectory tracking. Jie et al. [62] proposed a novel SMC approach with terminal SMC and sliding disturbance observer for controlling a hydraulic robot manipulator. To converge the tracking error to zero, a terminal SMS is applied, which exhibits a faster speed than conventional SMC. The proposed control compared with SMC; however, no results on resultant control effort is given. The mentioned works in this

section mainly considered the four important phenomena by using SMC or compound control methods: high tracking performance, robustness, convergence to zero in finite time, and chattering reduction.

Chapter 3

Control of MEMS gyroscope

3.1 Dynamics of MEMS gyroscope

A schematic of a typical z-axis MEMS gyroscope is presented in Figure 3.1. The traditional MEMS vibratory gyroscope design involves sensing mechanisms, a proof mass suspended by springs, and an electrostatic actuation system for forcing an oscillatory motion and sensing the position and velocity of the proof mass [63]. The proof mass is mounted on a frame, which moves with a constant linear velocity, while the gyroscope rotates at a slowly changing angular velocity Ω_z. The centrifugal forces $m\Omega_z^2 x$ and $m\Omega_z^2 y$ are supposed to be negligible due to small displacements x and y. The Coriolis forces, $2m\Omega_z^* \dot{y}$ and $2m\Omega_z^* \dot{x}$ are generated in a direction perpendicular to the drive and rotational axes [63].
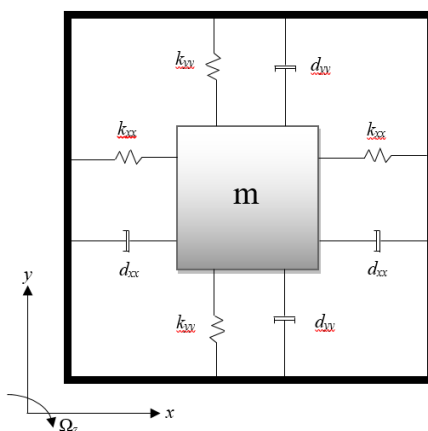
Figure 3.1 Schematic of MEMS gyroscope

The dynamics of the gyroscope is then governed by the following system of equations [63]:

$$m\ddot{x} + d_{xx}^* \dot{x} + d_{xy}^* \dot{y} + k_{xx}^* x + k_{xy}^* y = u_x^* + 2m\Omega_z^* \dot{y} \tag{3.1}$$

11

$$m\ddot{y} + d_{xy}^*\dot{y} + d_{yy}^*\dot{y} + k_{xy}^*x + k_{yy}^*y = u_y^* - 2m\Omega_z^*\dot{x} \tag{3.2}$$

In Eqs 1-2, x and y are coordinates with the origin at the center of the proof mass when no external force is applied. The coefficients k_{xy}^* and d_{xy}^* are the asymmetric spring and damping coefficients, respectively.

The spring constants of springs acting in the x- and y-directions, k_{xx}^*, k_{yy}^*, and damping rates d_{xx}^* and d_{yy}^* are often known; however, they may have small unknown variations from their nominal values [63], u_x^* and u_y^* are the control forces in the x and y-direction. The value of the proof mass m can be determined with high accuracy.

Eqs. (3.1), and (3.2) can be presented in the vector form as:

$$\frac{\ddot{q}^*}{q_0} + \frac{D^*}{m\omega_0}\frac{\dot{q}^*}{q_0} + \frac{K_a}{m\omega_0^2}\frac{q^*}{q_0} = \frac{u^*}{m\omega_0^2 q_0} - 2\frac{\Omega^*}{\omega_0}\frac{\dot{q}^*}{q_0} \tag{3.3}$$

where

$$q^* = \begin{bmatrix} x^* \\ y^* \end{bmatrix}, \quad u = \begin{bmatrix} u_x^* \\ u_y^* \end{bmatrix}, \quad \Omega* = \begin{bmatrix} 0 & -\Omega_z^* \\ \Omega_z^* & 0 \end{bmatrix}, D^* = \begin{bmatrix} d_{xx}^* & d_{xy}^* \\ d_{xy}^* & d_{yy}^* \end{bmatrix}, \quad K_a = \begin{bmatrix} k_{xx}^* & k_{xy}^* \\ k_{xy}^* & k_{yy}^* \end{bmatrix} \text{ and }$$

non-dimensional parameters [63]as follows:

$$q = \frac{q^*}{q_0}, \quad d_{xy} = \frac{d_{xy}^*}{m\omega_0}, \quad \Omega_z = \frac{\Omega_z^*}{\omega_0} \tag{3.4}$$

$$u = \frac{u_x^*}{m\omega_0^2 q_0}, \quad u_y = \frac{u_y^*}{m\omega_0^2 q_0} \tag{3.5}$$

$$\omega_x = \sqrt{\frac{k_{xx}}{m\omega_0^2}}, \quad \omega_y = \sqrt{\frac{k_{yy}}{m\omega_0^2}}, \quad \omega_{xy} = \frac{k_{xy}}{m\omega_0^2} \tag{3.6}$$

where q_0 is the reference length and ω_0 is the natural frequency of each axis. Finally, the dynamic equations for a MEMS gyroscope are-

$$\ddot{q} = -(D + 2\Omega)\dot{q} - K_b q + u + E \tag{3.7}$$

Where $E(N)$ is an external disturbance, which dynamic model can be presented as-

$$\ddot{q} = -Y\dot{q} - Pq + u + E \tag{3.8}$$

Where $Y=(D+2\Omega)$ and $P=K_b$. ΔY and ΔP determine some uncertainties of parameter variations. Thus, Eq. (3.8) can be denoted as:

Where,

$$q = \begin{bmatrix} x \\ y \end{bmatrix}, \quad u = \begin{bmatrix} u_x \\ u_y \end{bmatrix}, \quad \Omega = \begin{bmatrix} 0 & -\Omega_z \\ \Omega_z & 0 \end{bmatrix}$$

$$D = \begin{bmatrix} d_{xx} & d_{xy} \\ d_{xy} & d_{yy} \end{bmatrix}, \quad K_b = \begin{bmatrix} \omega_x^2 & \omega_{xy} \\ \omega_{xy} & \omega_y^2 \end{bmatrix}$$

we obtain,

$$\ddot{q} = -(Y + \Delta Y)\dot{q} - (P + \Delta P)q + u(t) + E \tag{3.9}$$

The Eq. (9) can be shown as:

$$\ddot{q} = -Y\dot{q} - Pq + u(t) + D(t) \tag{3.10}$$

where D(t) is as follows:

$$D(t) = -\Delta Y\dot{q} - \Delta Pq + E \tag{3.11}$$

3.2   Robust sliding mode control

Defining the tracking error as $e(t)=q_d(t)-q(t)$, q_d is the desired trajectory tracking; one can write the sliding mode surface as

$$s(t) = \dot{e}(t) + \gamma \int_0^t (sin(e(\tau)) + e^\beta(\tau))d\tau \tag{3.12}$$

where γ is a positive constant and β is a positive integer.

Differentiating the sliding mode surface concerning time and using Eq. (3.10) yields

$$\dot{s}(t) = \ddot{e}(t) + \gamma(sin(e(t)) + e^\beta(t))$$

$$= Y\dot{q} + Pq - u(t) - D(t) + \ddot{q}_d + \gamma(sin(e(t)) + e^\beta(t)) \tag{3.13}$$

The control effort is derived as the solution of $\dot{s}(t) = 0$ to achieve the desired performance under the nominal model. The equivalent control effort is defined as

$$u_{eq}(t) = -\ddot{q}_d - Y\dot{q} - Pq + D(t) - \gamma(sin(e(t)) + e^\beta(t)) \tag{3.14}$$

If unpredictable perturbations from the external disturbance or parameter variations occur, the equivalent control effort cannot guarantee favorable control performance. Thus, by designing an auxiliary control effort, the effect of unpredictable perturbations can be eliminated. For this purpose, stability analysis is performed. The Lyapunov function is defined as

$$V(t) = \frac{1}{2}s^T(t)s(t) \tag{3.15}$$

A sufficient stability condition for the control method is given by the requirement that the

Lyapunov function decreases at any time

$$\dot{V}(t) = s^T(t)\dot{s}(t) < 0 , \quad s(t) \neq 0 \tag{3.16}$$

Substitute Eq. (3.13) into Eq. (3.16) generates

$$\dot{V}(t) = s^T(t)(Y\dot{q} + Pq - u(t) - D(t) + \ddot{q}_d + \gamma(sin(e(t)) + e^{\beta}(t))) \tag{3.17}$$

The control input can be defined as:

$$u(t) = u_{RSMC}(t) = u_{eq}(t) + u_s(t) \tag{3.18}$$

Substitute Eq. (3.18) into Eq. (3.17) produces

$$\dot{V}(t) = s^T(t)(Y\dot{q} + Pq - u_{eq}(t) - u_s(t) - D(t) + \ddot{q}_d \tag{3.19}$$
$$+ \gamma(sin(e(t)) + e^{\beta}(t)))$$

Substitute Eq. (3.14) into Eq. (3.19) produces

$$\dot{V}(t) = s^T(t)(+Y\dot{q} + Pq - \ddot{q}_d - Y\dot{q} - Pq + D(t) - \gamma(sin(e(t)) + e^{\beta}(t)) \tag{3.20}$$
$$- u_s(t) - D(t) + \ddot{q}_d + \gamma(sin(e(t)) + e^{\beta}(t)))$$

Simplify Eq. (3.20) produces

$$\dot{V}(t) = s^T(t)(-u_s(t)) \tag{3.21}$$

The $u_s(t)$ can be defined as follows:

$$u_s(t) = K_s s(t) \tag{3.22}$$

Where $K_s=diag[K_{s1}, K_{s2}, \ldots\ldots, K_{sn}]$ is positive detfinite matrix and demonstrates reaching control gain.

By substituting Eq. (3.22) into Eq. (3.21), $\dot{V}(t) < 0$ will be observed.

3.3 New sliding mode control

It is well established that the essential and the most crucial part of SMC design is how to select SMS, which is provided to respond to desired control performance.

$$s(t) = \dot{e}(t) + \int_0^t (k_1 sig(e(t)) + k_2 sig(\dot{e}(t)))\, d\tau \tag{3.23}$$
$$where$$
$$sig(e(t)) = |e(t)|sign(e(t))$$
$$sig(\dot{e}(t)) = |\dot{e}(t)|sign(\dot{e}(t))$$

The SMC includes two crucial cases: equivalent control and reaching control law.

To obtain the equivalent controller, the SMS should be enforced to zero ($\dot{s}(t) = 0$) as:

$$\dot{s}(t) = \ddot{e}(t) + k_1 sig(e(t)) + k_2 sig(\dot{e}(t)) = 0 \tag{3.24}$$

Substitute $\ddot{e}(t) = \ddot{q}_d - \ddot{q}$ in Eq. (3.24) generates

$$\ddot{q}_d - \ddot{q} + k_1 sig(e(t)) + k_2 sig(\dot{e}(t)) = 0 \tag{3.25}$$

Substitute Eq. (3.10) into Eq. (3.25) produces

$$\ddot{q}_d + Y\dot{q} + Pq - u(t) - D(t) + k_1 sig(e(t)) + k_2 sig(\dot{e}(t)) = 0 \tag{3.26}$$

The equivalent control will be defined as:

$$u_{eq}(t) = \ddot{q}_d + Y\dot{q} + Pq - D(t) + k_1 sig(e(t)) + k_2 sig(\dot{e}(t)) \tag{3.27}$$

When external perturbations apply to the system, the equivalent control is enabled to suppress those noises. Thus, a second control law should be defined to be robust against external perturbations. The conventional reaching control law, which has been used in several types of

16

research [64, 65], will be selected according to Eq. (3.28). Note that the reaching control is implemented in most cases due to its robustness and high tracking performance.

$$u_s(t) = K_s s(t) \tag{3.28}$$

Where K_s is the positive constant. The proposed control input shows as:

$$u_{NSMC}(t) = u_{eq}(t) + u_s(t) \tag{3.29}$$

The Lyapunov theory is a strong tool for proving the stability of the proposed controller as:

$$V(t) = \frac{1}{2} s^T(t) s(t) \tag{3.30}$$

Take derivative from Eq. (3.30) generates

$$\dot{V}(t) = s^T(t)\dot{s}(t) < 0, \quad s(t) \neq 0 \tag{3.31}$$

When Eq. (3.31) satisfy, the control system will be stable. Substitute Eq. (3.24) into Eq. (3.31) produces:

$$\dot{V}(t) = s^T(t)(\ddot{e}(t) + k_1 sig(e(t)) + k_2 sig(\dot{e}(t))) \tag{3.32}$$

The Eq. (3.32) arranges as:

$$\dot{V}(t) = s^T(t)(\ddot{q}_d - \ddot{q} + k_1 sig(e(t)) + k_2 sig(\dot{e}(t))) \tag{3.33}$$

Substitute Eq. (3.10) into Eq. (3.33) produces

$$\dot{V}(t) = s^T(t)(\ddot{q}_d + Y\dot{q} + Pq - u(t) - D(t) + k_1 sig(e(t)) + k_2 sig(\dot{e}(t))) \tag{3.34}$$

Substitute Eq. (3.29) into Eq. (3.34) generates

$$\dot{V}(t) = s^T(t)(\ddot{q}_d + Y\dot{q} + Pq - u_{eq}(t) - u_s(t) - D(t) + k_1 sig(e(t)) \qquad (3.35)$$

$$+ k_2 sig(\dot{e}(t)))$$

Substitute Eq. (3.27) and Eq. (3.28) into Eq. (3.35) produces

$$\dot{V}(t) = s^T(t)(\ddot{q}_d + Y\dot{q} + Pq - \ddot{q}_d - Y\dot{q} - Pq + D(t) - k_1 sig(e(t)) \qquad (3.36)$$

$$- k_2 sig(\dot{e}(t)) - K_s s(t) - D(t) + k_1 sig(e(t)) + k_2 sig(\dot{e}(t)))$$

Simplify Eq. (3.36) produces

$$\dot{V}(t) = s^T(t)(-K_s s(t)) \qquad (3.37)$$

The Eq. (3.37) denotes as:

$$\dot{V}(t) = -K_s s(t)^2 \qquad (3.38)$$

The Eq. (3.38) satisfies $\dot{V}(t) < 0$. Therefore, the proposed control method is stable.

3.4 Fractional sliding mode control

FSMC is popular because of its robustness against external disturbances. The fractional-order sliding mode surface can be defined as follows:

$$s(t) = \dot{e}(t) + \lambda e(t) + \alpha D^\mu e(t) \qquad (3.39)$$

where α is a positive constant and μ is a fractional order operator [66].

Theorem 1: The derivation of fractional function [66]:

$$\frac{d}{dt}\left(D^\mu e(t)\right) = D^1 D^\mu e(t) = D^{\mu+1} e(t) = D^\mu \dot{e}(t)$$

The control system engineering can be considered as an important application of fractional order calculus. There are many definitions of fractional calculus, and they are used in various areas. The Grunwald-Letnikov fractional operator is well-known due to its myriad application in control system engineering.

The Grunwald-Letnikov fractional operator can be defined as follows [66]:

$$_aD_t^\mu = \lim_{h\to 0}\frac{1}{h^\mu}\sum_{r=0}^{\left[\frac{t-a}{h}\right]}(-1)^r \binom{n}{r}f(t-rh)$$

$$(3.40)$$

Where a and t are the limits of the operator and [t-a/h] is the integer part. n is the integer value that satisfies the condition n-$1<\mu<n$.

The value of the binomial coefficient is shown by

$$\binom{n}{r} = \frac{\Gamma(n+1)}{\Gamma(r+1)\Gamma(n-r+1)}$$

$$(3.41)$$

The Gamma function utilized in Eq. (3.41) can be defined as follows:

$$\Gamma(x) = \int_0^\infty t^{x-1}e^{-t}dt, \quad R(z) > 0$$

$$(3.42)$$

This definition is significantly appropriate in obtaining a numerical solution of fractional differential equations.

The equivalent FSMC is obtained by taking derivative of Eq. (3.39) as follows:

$$\dot{s}(t) = \ddot{e}(t) + \alpha D^{\mu+1}e(t) = \ddot{q}_d - \ddot{q} + \lambda\dot{e}(t) + \alpha D^{\mu+1}e(t) \qquad (3.43)$$

Substitute Eq. (3.10) into Eq. (3.43) produces

$$\dot{s}(t) = \ddot{q}_d + Y\dot{q} + Pq - u(t) - D(t) + \lambda\dot{e}(t) + \alpha D^{\mu+1}e(t) \tag{3.44}$$

Therefore, the equivalent control can be defined ($\dot{s}(t) = 0$):

$$u_{eq}(t) = \ddot{q}_d + Y\dot{q} + Pq - D(t) + \lambda\dot{e}(t) + \alpha D^{\mu+1}e(t) \tag{3.45}$$

When external disturbances apply to a system, the equivalent control cannot ensure the effectiveness of the control performance. As a result of this, an auxiliary control effort needs to be designed in order to compensate for the effect of the external disturbances. The Lyapunov function can be chosen for this task as follows:

$$V(t) = \frac{1}{2}s^T(t)s(t) \tag{3.46}$$

To guarantee the stability of the control method, an appropriate condition should be selected as follows:

$$\dot{V}(t) = s^T(t)\dot{s}(t) < 0, \quad s(t) \neq 0 \tag{3.47}$$

To satisfy the reaching condition, the equivalent control $u_{eq}(t)$ given in Eq. (3.45) is completed by a control term.

$$u(t) = u_{FSMC}(t) = u_{eq}(t) + u_s(t) \tag{3.48}$$

The Lyapunov theory is a strong tool for proving the stability of the proposed controller as:

$$V(t) = \frac{1}{2}s^T(t)s(t) \tag{3.49}$$

Take derivative from Eq. (3.49) generates

$$\dot{V}(t) = s^T(t)\dot{s}(t) < 0 , \quad s(t) \neq 0 \tag{3.50}$$

When the Eq. (3.50) satisfy, the control system will be stable. Substitute Eq. (3.44) into Eq. (3.50) produces:

$$\dot{V}(t) = s^T(t)(\ddot{q}_d + Y\dot{q} + Pq - u(t) - D(t) + \lambda\dot{e}(t) + \alpha D^{\mu+1}e(t)) \tag{3.51}$$

Substitute Eq. (3.48) into Eq. (3.51) generates

$$\dot{V}(t) = s^T(t)(\ddot{q}_d + Y\dot{q} + Pq - u_{eq}(t) - u_s(t) - D(t) + \lambda\dot{e}(t) + \alpha D^{\mu+1}e(t)) \tag{3.52}$$

Substitute Eq. (3.28) and Eq. (3.45) into Eq. (3.52) produces

$$\dot{V}(t) = s^T(t)(\ddot{q}_d + Y\dot{q} + Pq - \ddot{q}_d - Y\dot{q} - Pq + D(t) - \lambda\dot{e}(t) - \alpha D^{\mu+1}e(t) \tag{3.53}$$
$$- K_s s(t) - D(t) + \lambda\dot{e}(t) + \alpha D^{\mu+1}e(t))$$

Simplify Eq. (3.53) produces

$$\dot{V}(t) = s^T(t)(-K_s s(t)) \tag{3.54}$$

The Eq. (3.54) denotes as:

$$\dot{V}(t) = -K_s s(t)^2 \tag{3.55}$$

The Eq. (3.55) satisfies $\dot{V}(t) < 0$. Therefore, the proposed control method is stable.

3.5   Simulation results
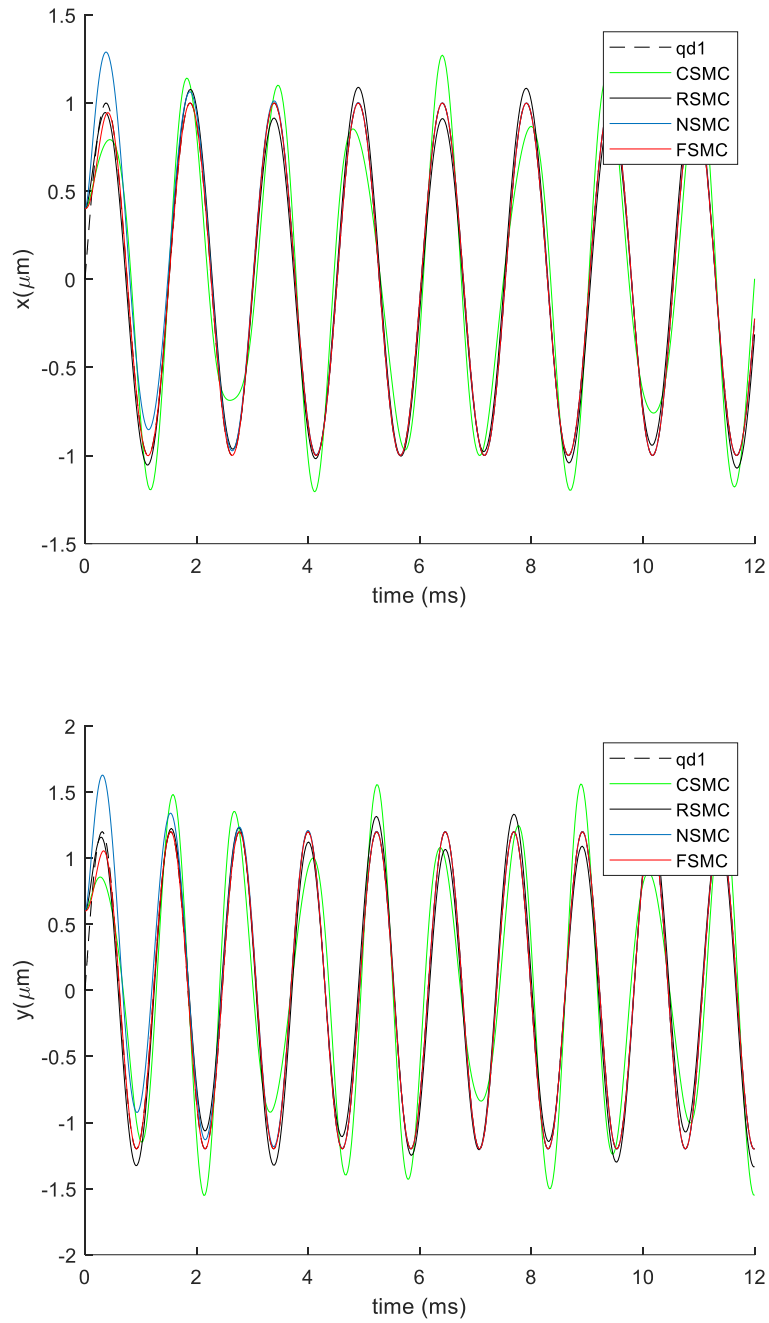
Figure *3*.2 Position tracking of x-axis and y-axis under CSMC, RSMC, NSMC, and FSMC.

Numerical simulations were performed to demonstrate the performance of the proposed controllers. The RSMC, NSMC, and FSMC parameters are chosen as γ=5, β=4, K_1=10, K_2=10,
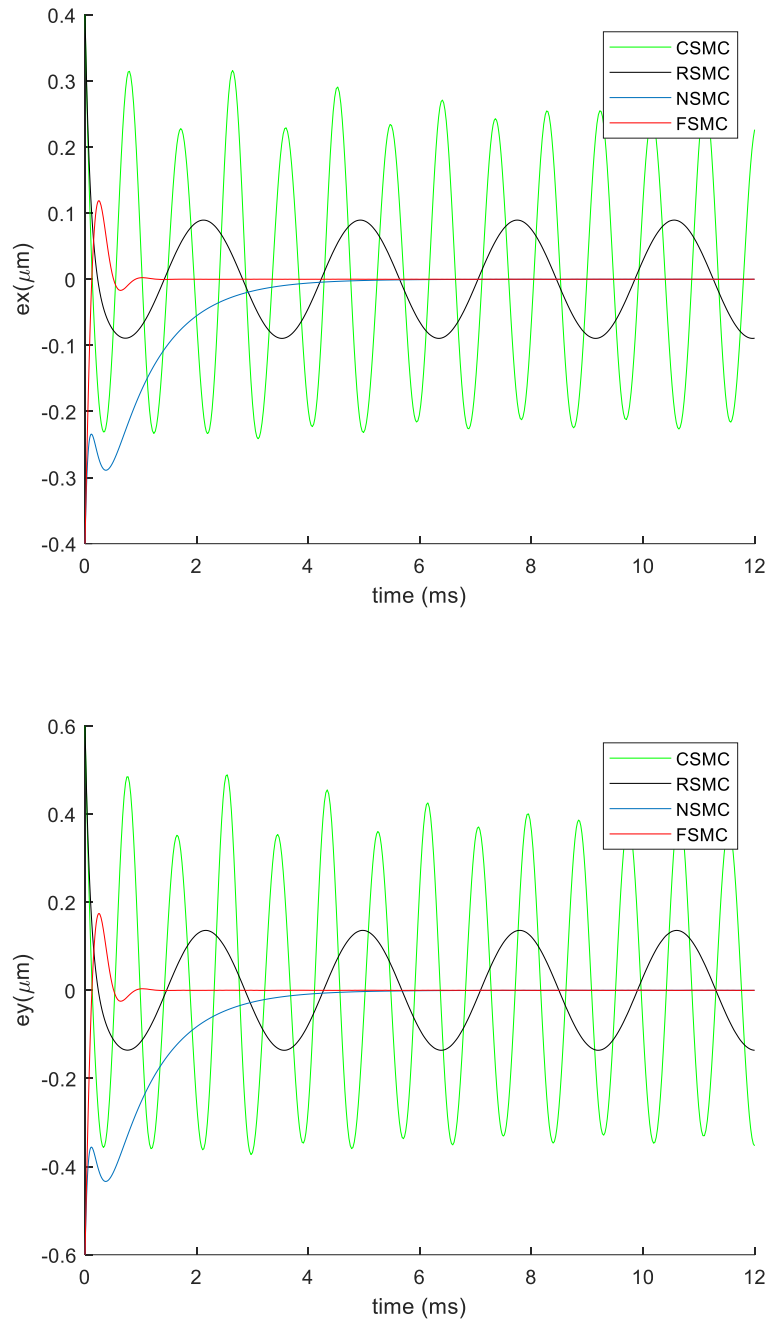
Figure *3*.3 Position tracking error of x-axis and y-axis under CSMC, RSMC, NSMC, and FSMC.

λ=10, α=50, and μ=0.5 by trial and error to obtain suitable results. The sliding surface is selected as *K$_s$=diag(10,10)*. The desired motion trajectory is determined by *q$_{d1}$=sin (4.17t)*, and

$q_{d2}=1.2sin(5.11t)$. The initial values of the system are selected as $q_1(0) = 0.4$, $q_2(0) = 0.6$, $\dot{q}_1(0) = 0$ and $\dot{q}_2(0) = 0$. The initial parameters are selected by trial and error to improve tracking performance of the proposed control method in the x and y directions.

The parameters of the MEMS gyroscope are selected as [67]:

$$m = 1.8 \times 10^{-7}kg \qquad k_{xy} = 12.779N/m \qquad d_{xy} = 3.6 \times 10^{-7}Ns/m$$

$$k_{xx} = 63.955N/m \qquad d_{xx} = 1.8 \times 10^{-6}Ns/m$$

$$k_{yy} = 95.92N/m \qquad d_{yy} = 1.8 \times 10^{-6}Ns/m$$

When the displacement range of the MEMS gyroscope in each axis is in the sub-micrometer level, it is convenient to choose q_0=1 μm as the reference length [63]. When the ω_0 is selected as 1 kHz, the common natural frequency of each axis of a MEMS gyroscope is in the kHz range. The unknown angular velocity is assumed as Ω_z=100 rad/s [63]. Therefore, the nondimensional values of the MEMS gyroscope parameters are chosen as [63]:

$$\omega_x^2 = 355.3, \ \omega_y^2 = 532.9, \ \omega_{xy} = 70.99, \ d_{xx} = 0.01, \ d_{yy} = 0.01, \ d_{xy} = 0.002, \ \Omega_z = 0.1$$

Figure 3.2 illustrates the MEMS gyroscope motion along the x and y axes. The trajectory tracking was performed using a CSMC, an RSMC, an NSMC, and an FSMC. It can be observed that the actual motion trajectory of the MEMS gyroscope is consistent with the desired reference trajectory, showing that the tracking performance of FSMC is better in comparison with CSMC, RSMC, and NSMC. The tracking errors corresponding to the trajectory tracking shown in Figure 3.2 are plotted in Figure 3.3. The results in Figure 3.3 also show that FSMC effectively reduces oscillation which was observed in CSMC. Moreover, the FSMC results in faster convergence (see Figure 3.3).
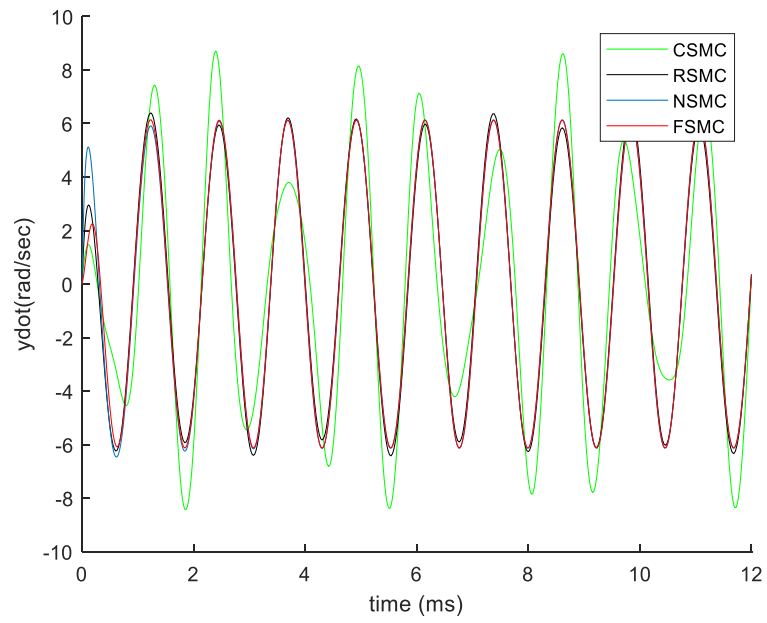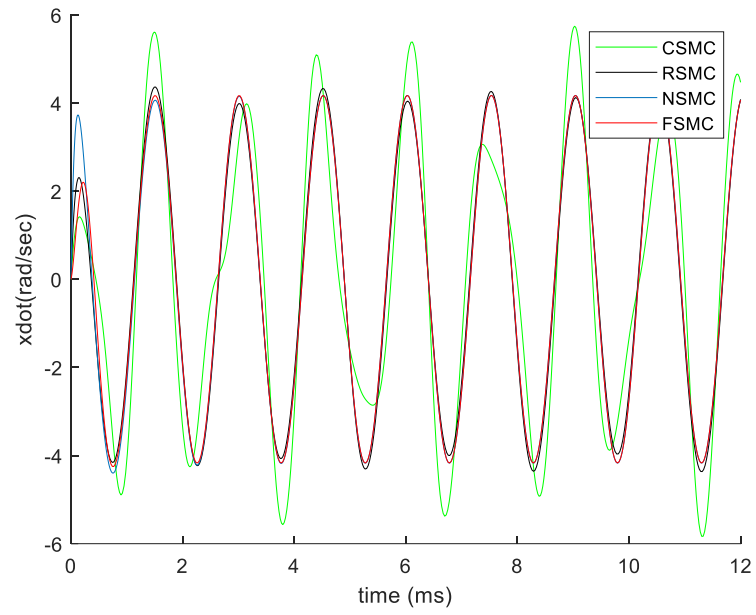
Figure *3*.4. Velocity in x-axis and y-axis under CSMC, RSMC, NSMC and FSMC.
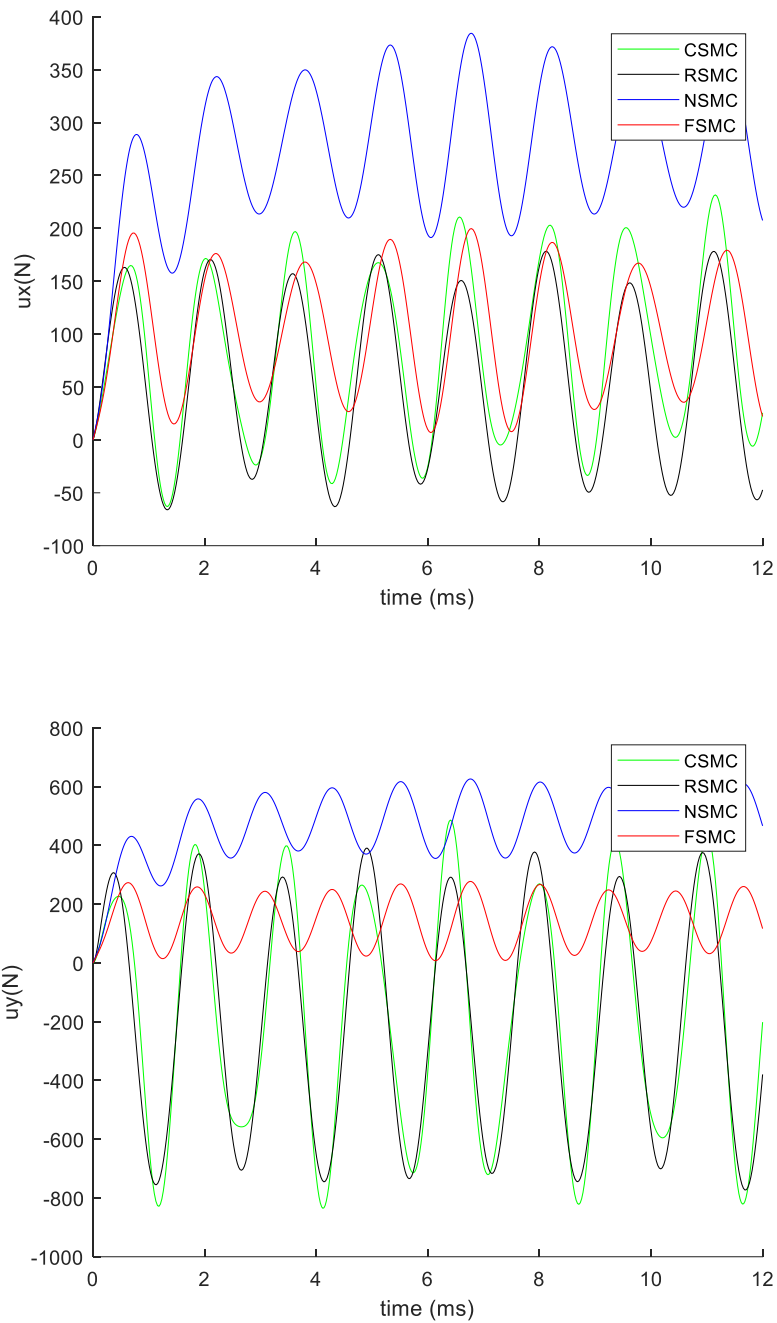
Figure *3*.5. Control effort using CSMC, RSMC, NSMC and FSMC.

The velocities along *x* and *y*-axes corresponding to the trajectory shown in Figure 3.2 are illustrated in Figure 3.4, whereas, Figure 3.5 demonstrates the control efforts of CSMC, RSMC,

NSMC, and FSMC, which the FSMC is smoother than CSMC and RSMC. Therefore, the oscillation phenomenon has been reduced in FSMC.

3.5.1   Robustness testing: random noise suppression

A robust controller is expected to suppress the external disturbances . In the simulation, we applied random noise (as an external disturbance, $D(t) = 0.5\ randn(1,1)$) with a standard deviation of 0.05 to test the noise suppression ability of the proposed controller. Figure 3.6 shows the simulation results, where it is evident that FSMC can suppress the external disturbances.
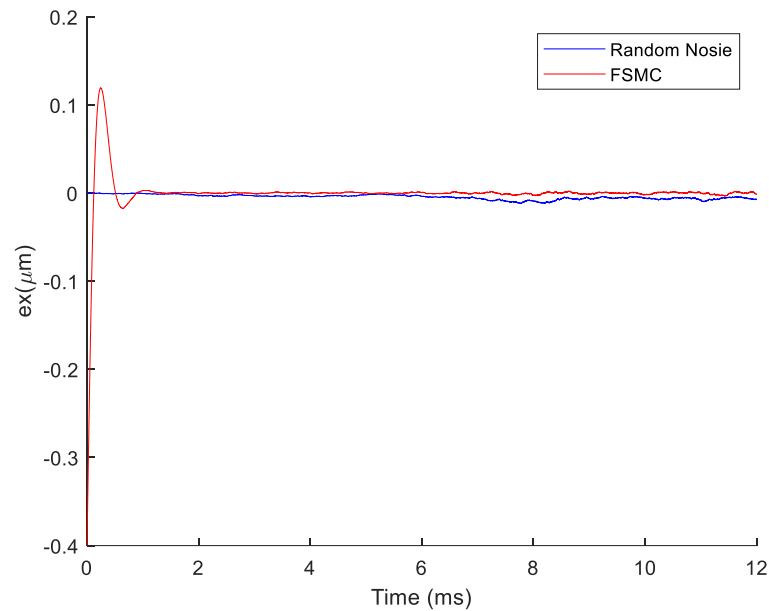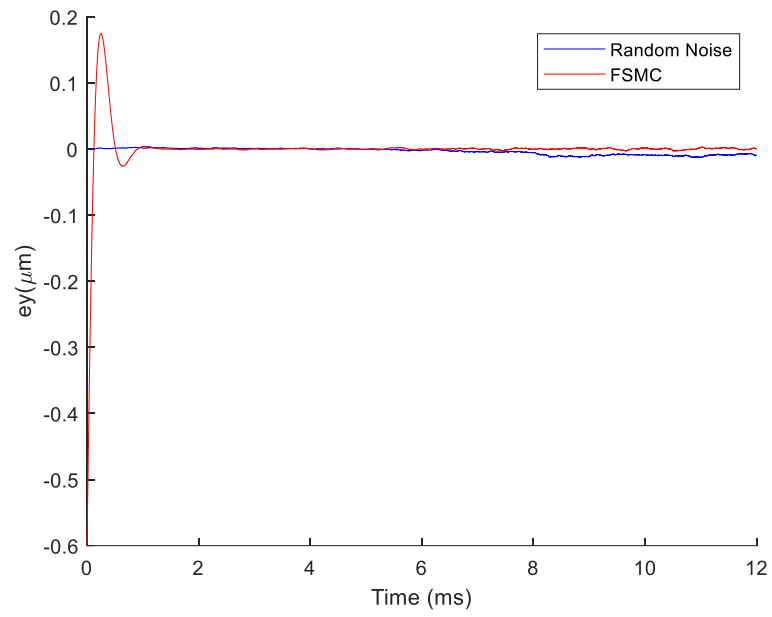
Figure 3.6 Robustness verification of FSMC under random noise application.

Chapter 4

Control of an Exoskeleton Robot

and a 2 DoFs Robot Manipulator

4.1 Dynamic model of an exoskeleton robot

The robot, as shown in Figure 4.1 is an exoskeleton type robot designed to be worn on the lateral side of the human upper limb. Mass and inertia properties of this robot are given in Appendix B.

Table 4.1 Workspace ETS-Marse [68]

Joints	Motion	Range of Motion
1	Shoulder joint horizontal flexion/extension	$0°/180°$
2	Shoulder joint vertical flexion/extension	$180°/0°$
3	Shoulder joint internal/external rotation	$90°/90°$
4	Elbow joint flexion/extension	$145°/0°$
5	Forearm joint pronation/supination	$90°/90°$
6	Wrist joint ulnar/radial deviation	$30°/20°$
7	Wrist joint flexion/extension	$60°/50°$
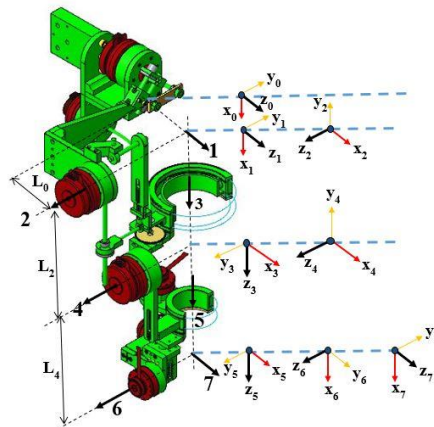
Figure 4.1 Reference frames of exoskeleton robot [68].

The key design features of exoskeleton robot include convenient power/weight ratio, easy fitting and removal, low weight, and capability of compensating for gravity. DH-parameters and

Table 4.2. DH parameters [68].

Joint (i)	Joint Name	α_{i-1} (Link twist)	a_{i-1} (Link length)	d_i (Link offset)	q_i (Joint variable)
1	Abduction/ adduction	0	0	L_0	q_1
2	Vertical Flexion/extension	$\pi/2$	0	0	$q_2 + \pi/2$
3	Internal/external rotation	$\pi/2$	0	L_2	q_3
4	Elbow Flexion/extension	$-\pi/2$	0	0	q_4
5	Pronation/ Supination	$\pi/2$	0	L_4	q_5
6	Wrist Radial/ulnar deviation	$-\pi/2$	0	0	$q_6 - \pi/2$
7	Wrist Flexion/Extension	$-\pi/2$	0	0	q_7

workspace is shown in Table 4.1 and Table 4.2, respectively.

The exoskeleton robot can perform passive therapeutic motion (i.e., completely hold and support the subject's upper limb provide therapeutic motion), active assistive motion (where subject actively participates in the therapeutic sessions and the robot assist the subject when it needs). The characteristics of the exoskeleton robot and its dynamic model are completely outlined in [69-72], which can be summarized as:

$$M(\theta)\ddot{\theta} + C(\theta,\dot{\theta})\dot{\theta} + G(\theta) + F(\theta,\dot{\theta}) = \tau \tag{4.1}$$

Where $q, \dot{q}, \ddot{q} \in R^{7\times1}$ illustrates the position, velocity, and acceleration of the joints, respectively. Also, in the dynamic model of the 7DoFs robot manipulator, $M(q) \in R^{7\times7}$ represented as the inertia matrix, $C(q,\dot{q}) \in R^{7\times1}$ known as the vector of centrifugal and

Coriolis forces, $G(q) \in R^{7\times1}$ is a gravitational vector, and $\tau \in R^{7\times1}$ the joint torques.

Eq. (4.1) can be shown as:

$$\ddot{\theta} = -P\dot{\theta} - QG - QF + u(t) \tag{4.2}$$

Where, $P = M^{-1}(\theta)C(\theta, \dot{\theta}), = M^{-1}(\theta)$, and $u(t) = Q\tau$.

4.2 Dynamic model of a 2 DoFs robot manipulator

Robotics manipulator is widely applicable in different fields such as industrial robots, biorobotics, and aerospace robots. The mechanism of the proposed two degrees of freedom (2 DoFs) robot manipulator is illustrated in Figure 4.2.

Figure 4.3 shows the schematic of the robotic manipulator. The dynamic modeling of a 2DoFs robot arm is as follows [76]:

$$M(q)\ddot{q} + N(q, \dot{q})\dot{q} + G(q) = \tau \tag{4.3}$$

Where $q, \dot{q}, \ddot{q} \in R^{2\times1}$ illustrates the position, velocity, and acceleration of the joints, respectively. Also, in the dynamic model of the 2DoFs robot manipulator, $M(q) \in R^{2\times2}$ represented as the inertia matrix, $N(q, \dot{q}) \in R^{2\times1}$ known as the vector of centrifugal and Coriolis forces, $G(q) \in R^{2\times1}$ is a gravitational vector, and $\tau \in R^{2\times1}$ the joint torques. $M(q), N(q, \dot{q}), G(q)$ and are provided in Appendix A.

Figure *4.*2 Robot manipulator.
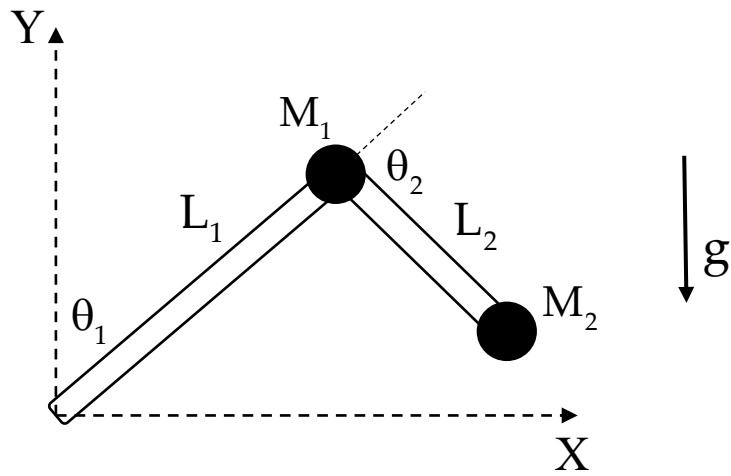
Figure *4.*3 Structure of robot manipulator.

Eq. (4.3) can be shown as:

$$\ddot{\theta} = -P\dot{\theta} - QG - QF + u(t) \qquad (4.4)$$

Where, $P = M^{-1}(\theta)N(\theta,\dot{\theta})$, $= M^{-1}(\theta)$, and $u(t) = Q\tau$.

4.3 Control of an Exoskeleton robot and a 2 DoFs robot manipulator

4.3.1 Robust sliding mode control (RSMC)

Complex systems always need a stable control system to compensate unmodeled dynamic uncertainties and robust against external disturbances. By using a sliding mode controller (SMC), the system states can be guaranteed to reach a sliding mode switching surface in finite-time and converge to the origin in finite time.

The proposed robust sliding mode switching function can be defined as follows:

$$s(t) = \dot{e}(t) + \gamma \int_0^t (sin(e(\tau)) + e^\beta(\tau))d\tau \qquad (4.5)$$

By using a robust sliding mode switching function, the tracking error converges to zero in finite time.

The gain parameters of RSMC are known as γ and β is the fractional order operator. The tracking error can be shown as:

$$e(t) = \theta_d - \theta \qquad (4.6)$$

where θ_d is the desired trajectory. The equivalent control can be obtained as:

$$\dot{s}(t) = \ddot{e}(t) + \gamma(sin(e(t)) + e^\beta(t)) = \ddot{\theta}_d - \ddot{\theta} + \gamma(sin(e(t)) + e^\beta(t)) \qquad (4.7)$$

The Eq. (4.8) can be obtained by substituting Eq. (4.2) into Eq. (4.7)

$$\dot{s}(t) = \ddot{\theta}_d + P\dot{\theta} + QG + QF - u(t) + \gamma(sin(e(t)) + e^\beta(t)) \qquad (4.8)$$

The control effort is derived as the solution of $\dot{s}(t) = 0$.

The control effort can be obtained as:

$$u_{eq}(t) = \ddot{\theta}_d + P\dot{\theta} + QG + QF + \gamma(sin(e(t)) + e^{\beta}(t)) \tag{4.9}$$

The equivalent control effort cannot guarantee the desired performance because unpredictable perturbations from external disturbances or parameter variations occur. Consequently, a second controller should be added to suppress the effect of external disturbances. The Lyapunov function can be selected for this issue as:

$$V(t) = \frac{1}{2}s^T(t)s(t) \tag{4.10}$$

Stability condition can be defined as [73-75]:

$$\dot{V}(t) = s^T(t)\dot{s}(t) < 0, \quad s(t) \neq 0 \tag{4.11}$$

The control scheme can be defined as:

$$u(t) = u_{RSMC}(t) = u_{eq}(t) + u_s(t) \tag{4.12}$$

To obtain the reaching control law $u_s(t)$ [75], Eq. (4.11) is shown as follows:

$$\dot{V}(t) = s^T(\ddot{\theta}_d - \ddot{\theta} + \gamma(sin(e(t)) + e^{\beta}(t))) \tag{4.13}$$

Substitute Eq. (4.2) into Eq. (4.13) produces

$$\dot{V}(t) = s^T(\ddot{\theta}_d + P\dot{\theta} + QG + QF - u(t) + \gamma(sin(e(t)) + e^{\beta}(t))) \tag{4.14}$$

By substituting Eq. (4.8) into Eq. (4.14), it can be shown as:

$$\dot{V}(t) = s^T(\ddot{\theta}_d + P\dot{\theta} + QG + QF - u_{eq}(t) - u_s(t) + \gamma(sin(e(t)) + e^{\beta}(t))) \tag{4.15}$$

By substituting Eq. (4.9) into Eq. (4.15), it can be shown as

$$\dot{V}(t) = s^T(\ddot{\theta}_d + P\dot{\theta} + QG + QF - \ddot{\theta}_d - P\dot{\theta} - QG - QF$$

$$-\gamma(sin(e(t)) + e^{\beta}(t)) - u_s(t) + \gamma(sin(e(t)) + e^{\beta}(t))) \tag{4.16}$$

Simplify Eq. (4.16) generates

$$\dot{V}(t) = s^T(-u_s(t)) \tag{4.17}$$

The reaching control can be chosen as:

$$u_s(t) = K_s s(t) \tag{4.18}$$

Where K_s is a positive constant. Substitute Eq. (4.18) into Eq. (4.17) produces

$$\dot{V}(t) = s^T\left(-K_s s(t)\right) = -K_s s^2(t) < 0 \tag{4.19}$$

Consequently, it can be observed from Eq. (4.19) that $\dot{V}(t) < 0$.

4.3.2 New sliding mode control

The sliding mode surface can be defined as:.

$$s(t) = \dot{e}(t) + \int_0^t (k_1 sig(e(t)) + k_2 sig(\dot{e}(t)))\, d\tau \tag{4.20}$$
$$where$$
$$sig(e(t)) = |e(t)|sign(e(t))$$
$$sig(\dot{e}(t)) = |\dot{e}(t)|sign(\dot{e}(t))$$

The SMC contains two parts: equivalent control and reaching control law.

The SMS should be enforced to zero ($\dot{s}(t) = 0$) to obtain the equivalent controller as:

$$\dot{s}(t) = \ddot{e}(t) + k_1 sig(e(t)) + k_2 sig(\dot{e}(t)) = 0 \tag{4.21}$$

Substitute $\ddot{e}(t) = \ddot{\theta}_d - \ddot{\theta}$ in Eq. (4.21) generates

$$\ddot{\theta}_d - \ddot{\theta} + k_1 sig(e(t)) + k_2 sig(\dot{e}(t)) = 0 \tag{4.22}$$

Substitute Eq. (4.2) into Eq. (4.22) produces

$$\ddot{\theta}_d + P\dot{\theta} + QG + QF - u(t) + k_1 sig(e(t)) + k_2 sig(\dot{e}(t)) = 0 \tag{4.23}$$

The equivalent control will be defined as:

$$u_{eq}(t) = \ddot{\theta}_d + P\dot{\theta} + QG + QF + k_1 sig(e(t)) + k_2 sig(\dot{e}(t)) \tag{4.24}$$

When external perturbations apply to the system, the equivalent control is enabled to suppress those noises. Thus, a second control law should be defined to be robust against external perturbations. The conventional reaching control law, which has been used in several types of research, will be selected according to Eq. (4.25). The reasons why reaching control is implemented in most cases are its robustness and high tracking performance.

$$u_s(t) = K_s s(t) \tag{4.25}$$

Where K_s is a positive constant. The proposed control input shows as:

$$u_{NSMC}(t) = u_{eq}(t) + u_s(t) \tag{4.26}$$

The Lyapunov theory is a strong tool for proving the stability of the proposed controller as:

$$V(t) = \frac{1}{2}s^T(t)s(t) \tag{4.27}$$

Take derivative from Eq. (4.27) generates (stability condition)

$$\dot{V}(t) = s^T(t)\dot{s}(t) < 0, \quad s(t) \neq 0 \tag{4.28}$$

When the Eq. (4.28) satisfy, the control system will be stable. Substitute Eq. (4.21) into Eq.

36

(4.28) produces:

$$\dot{V}(t) = s^T(t)(\ddot{e}(t) + k_1 sig(e(t)) + k_2 sig(\dot{e}(t))) \qquad (4.29)$$

The Eq. (4.29) arranges as:

$$\dot{V}(t) = s^T(t)(\ddot{\theta}_d - \ddot{\theta} + k_1 sig(e(t)) + k_2 sig(\dot{e}(t))) \qquad (4.30)$$

Substitute Eq. (4.2) into Eq. (4.30) produces

$$\dot{V}(t) = s^T(t)(\ddot{\theta}_d + P\dot{\theta} + QG + QF - u(t) + k_1 sig(e(t)) + k_2 sig(\dot{e}(t))) \qquad (4.31)$$

Substitute Eq. (4.26) into Eq. (4.31) generates

$$\dot{V}(t) = s^T(t)(\ddot{\theta}_d + P\dot{\theta} + QG + QF - u_{eq}(t) - u_s(t) + k_1 sig(e(t)) \qquad (4.32)$$
$$+ k_2 sig(\dot{e}(t)))$$

Substitute Eq. (4.24) and Eq. (4.25) into Eq. (4.32) produces

$$\dot{V}(t) = s^T(t)(\ddot{\theta}_d + P\dot{\theta} + QG + QF - \ddot{\theta}_d - P\dot{\theta} - QG - QF - k_1 sig(e(t)) \qquad (4.33)$$
$$- k_2 sig(\dot{e}(t)) - K_s s(t) + k_1 sig(e(t)) + k_2 sig(\dot{e}(t)))$$

Simplify Eq. (4.33) produces

$$\dot{V}(t) = s^T(t)(-K_s s(t)) \qquad (4.34)$$

The Eq. (4.34) denotes as:

$$\dot{V}(t) = -K_s s(t)^2 \qquad (4.35)$$

The Eq. (4.35) satisfies $\dot{V}(t) < 0$. Therefore, the proposed control method is stable.

4.3.3 Fractional sliding mode control

FSMC is popular because of its robustness against external disturbances. The fractional-order sliding mode surface can be defined as follows:

$$s(t) = \dot{e}(t) + \lambda e(t) + \alpha D^{\mu} e(t) \tag{4.36}$$

where α is a positive constant and μ is a fractional order operator [66].

Theorem 1: The derivation of fractional function [66]:

$$\frac{d}{dt}\left(D^{\mu}e(t)\right) = D^{1}D^{\mu}e(t) = D^{\mu+1}e(t) = D^{\mu}\dot{e}(t)$$

The control system engineering can be considered as an important application of fractional order calculus.

There are many definitions of fractional calculus, and each of them has mostly been used in some specific area. The Grunwald-Letnikov fractional operator is well-known due to its myriad application in control system engineering.

The Grunwald-Letnikov fractional operator can be defined as follows [66]:

$$_{a}D_{t}^{\mu} = \lim_{h \to 0} \frac{1}{h^{\mu}} \sum_{r=0}^{\left[\frac{t-a}{h}\right]} (-1)^{r} \binom{n}{r} f(t - rh) \tag{4.37}$$

Where *a* and *t* are the limits of operator and [*t-a/h*] is the integer part. *n* is the integer value which satisfies the condition *n-1<μ<n*.

The value of the binomial coefficient is shown by

$$\binom{n}{r} = \frac{\Gamma(n+1)}{\Gamma(r+1)\Gamma(n-r+1)}$$

(4.38)

The Gamma function utilized in Eq. (4.38) can be defined as follows:

$$\Gamma(x) = \int_0^\infty t^{x-1}e^{-t}dt, \quad R(z) > 0$$

(4.39)

This definition is significantly appropriate in obtaining a numerical solution of fractional differential equations.

The equivalent FSMC is obtained by taking derivative of Eq. (4.36) as follows:

$$\dot{s}(t) = \ddot{e}(t) + \alpha D^{\mu+1}e(t) = \ddot{\theta}_d - \ddot{\theta} + \lambda\dot{e}(t) + \alpha D^{\mu+1}e(t)$$

(4.40)

Substitute Eq. (4.2) into Eq. (4.40) produces

$$\dot{s}(t) = \ddot{\theta}_d + P\dot{\theta} + QG + QF - u(t) + \lambda\dot{e}(t) + \alpha D^{\mu+1}e(t)$$

(4.41)

Therefore, the equivalent control can be defined ($\dot{s}(t) = 0$):

$$u_{eq}(t) = \ddot{\theta}_d + P\dot{\theta} + QG + QF + \lambda\dot{e}(t) + \alpha D^{\mu+1}e(t)$$

(4.42)

When external disturbances apply on a system, the equivalent control cannot ensure the effectiveness of the control performance. As a result of this, auxiliary control effort needs to be designed in order to compensate for the effect of the external disturbances. The Lyapunov function can be chosen for this task as follows:

$$V(t) = \frac{1}{2}s^T(t)s(t)$$

(4.43)

In order to guarantee the stability of the control method, an appropriate condition should be

selected as follows:

$$\dot{V}(t) = s^T(t)\dot{s}(t) < 0, \quad s(t) \neq 0 \tag{4.44}$$

In order to satisfy the reaching condition, the equivalent control $u_{eq}(t)$ given in Eq. (4.42) is completed by a control term.

$$u(t) = u_{FSMC}(t) = u_{eq}(t) + u_s(t) \tag{4.45}$$

The Lyapunov theory is a strong tool for proving the stability of the proposed controller as:

$$V(t) = \frac{1}{2}s^T(t)s(t) \tag{4.46}$$

Take derivative from Eq. (4.46) generates

$$\dot{V}(t) = s^T(t)\dot{s}(t) < 0 , \quad s(t) \neq 0 \tag{4.47}$$

When the Eq. (4.47) satisfy, the control system will be stable. Substitute Eq. (4.41) into Eq. (4.47) produces:

$$\dot{V}(t) = s^T(t)(\ddot{\theta}_d + P\dot{\theta} + QG + QF - u(t) + \lambda\dot{e}(t) + \alpha D^{\mu+1}e(t)) \tag{4.48}$$

Substitute Eq. (4.45) into Eq. (4.48) generates

$$\dot{V}(t) = s^T(t)(\ddot{\theta}_d + P\dot{\theta} + QG + QF - u_{eq}(t) - u_s(t) + \lambda\dot{e}(t) + \alpha D^{\mu+1}e(t)) \tag{4.49}$$

Substitute Eq. (4.25) and Eq. (4.42) into Eq. (4.49) produces

$$\dot{V}(t) = s^T(t)(\ddot{\theta}_d + P\dot{\theta} + QG + QF - \ddot{\theta}_d - P\dot{\theta} - QG - QF - \lambda\dot{e}(t) \tag{4.50}$$
$$- \alpha D^{\mu+1}e(t) - K_s s(t) + \lambda\dot{e}(t) + \alpha D^{\mu+1}e(t))$$

Simplify Eq. (4.50) produces

$$\dot{V}(t) = s^T(t)(-K_s s(t)) \qquad (4.51)$$

The Eq. (4.51) denotes as:

$$\dot{V}(t) = -K_s s(t)^2 \qquad (4.52)$$

The Eq. (4.52) satisfies $\dot{V}(t) < 0$. Therefore, the proposed control method is stable.

4.4 Simulation results

4.4.1 Exoskeleton robot

The MATLAB software was used to simulate the proposed control methods (solver used: ode45).

Simulation Parameters:

The NSMC parameters are: K_1=1000 and K_2=1000,

The FSMC parameters are: λ=10, α=15, and μ=0.5, and K_s =40.

The parameters are chosen by trial and error to obtain suitable results.

Figure 4.4 illustrates the trajectory tracking of the robot joints under CSMC, NSMC, and FSMC. The tracking errors of joints corresponding to the trajectories shown in Fig.4.4 are plotted in Figure 4.5.
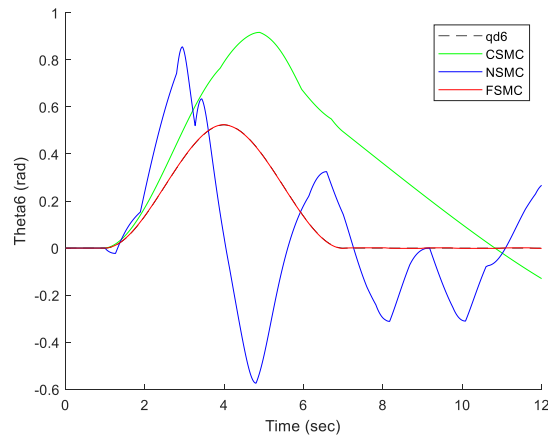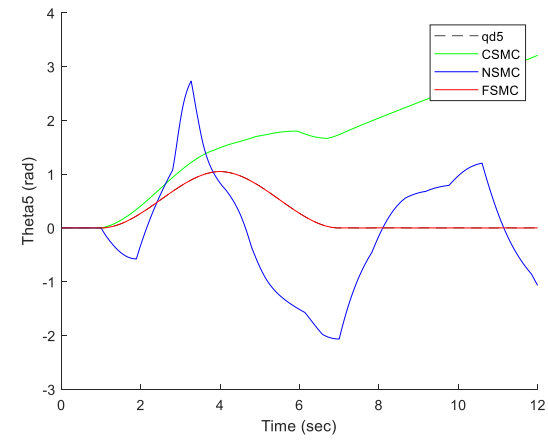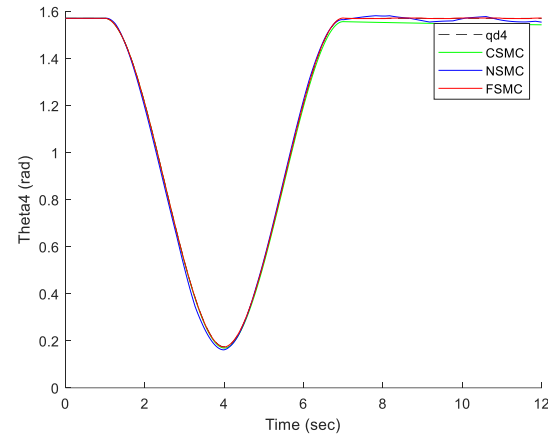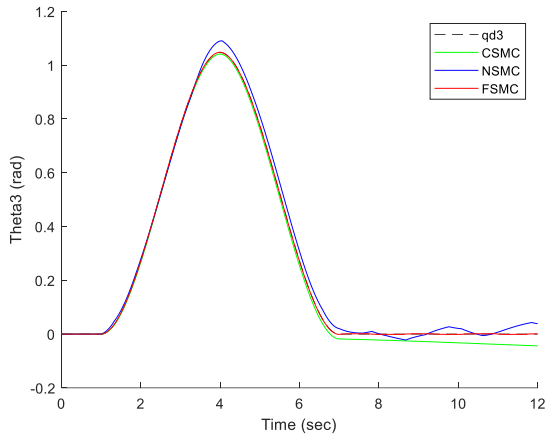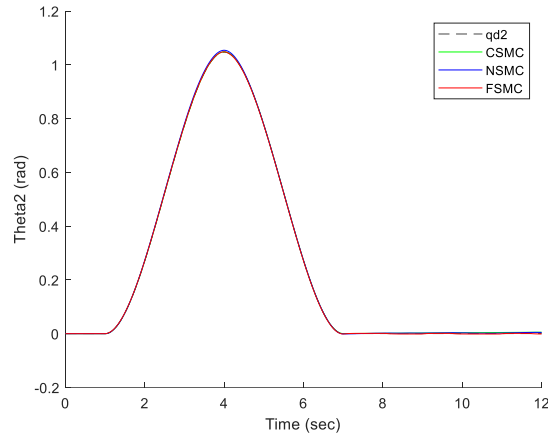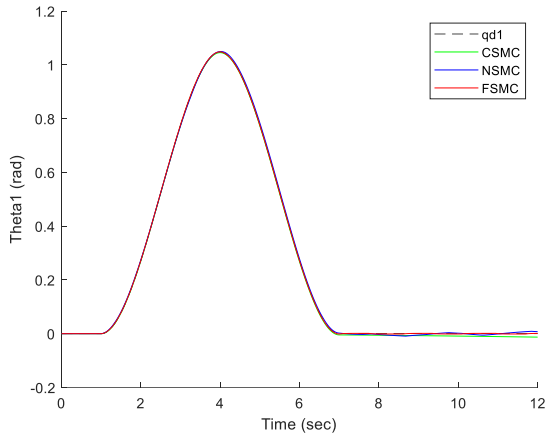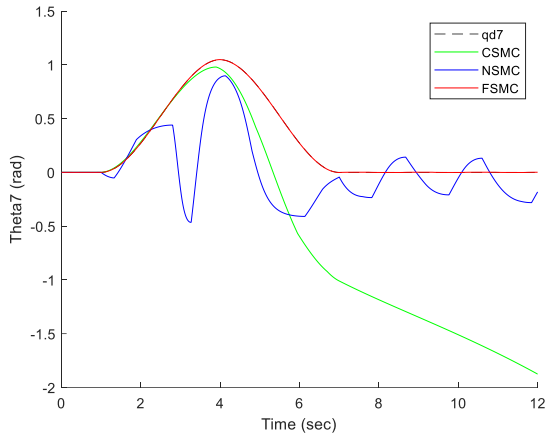
Figure *4*.4 Position tracking of joints under CSMC, NSMC, and FSMC.
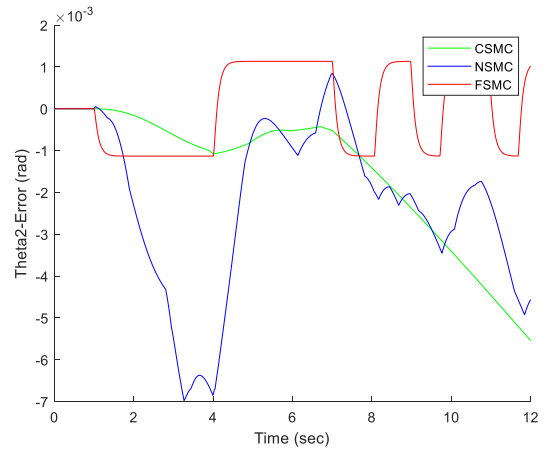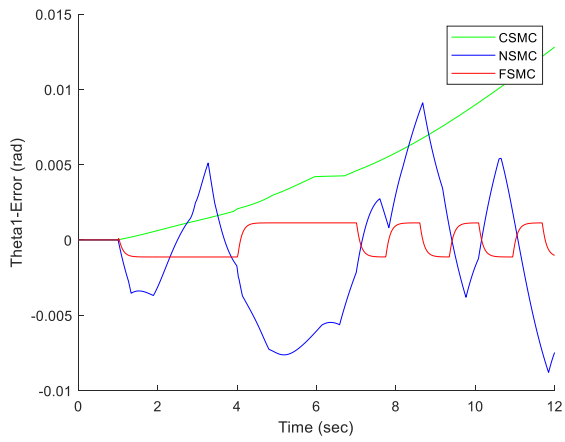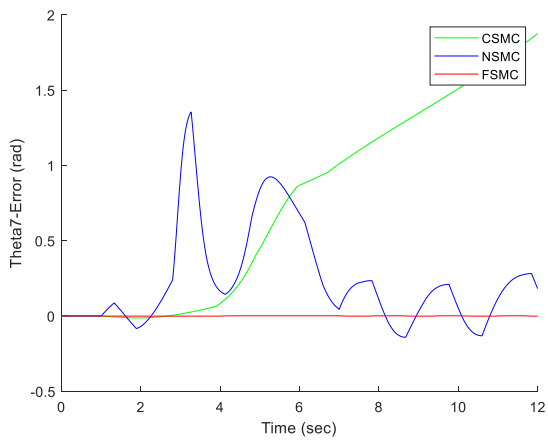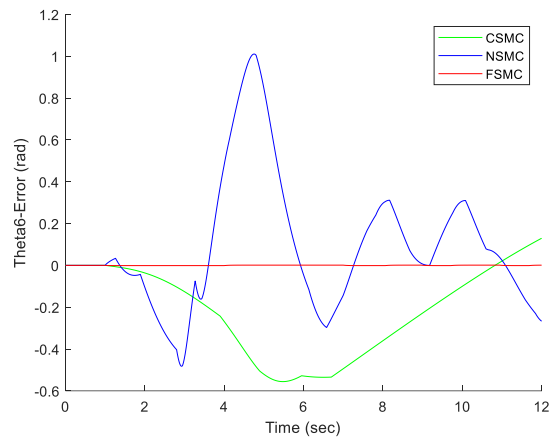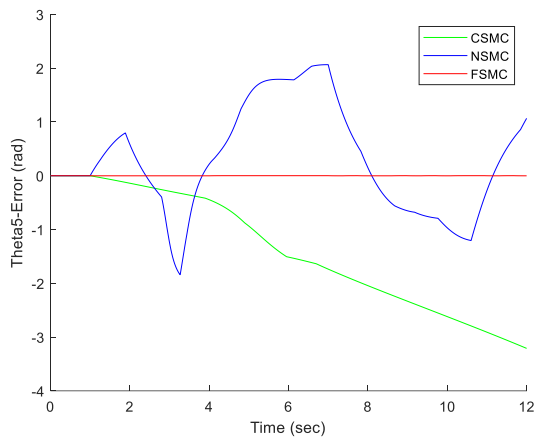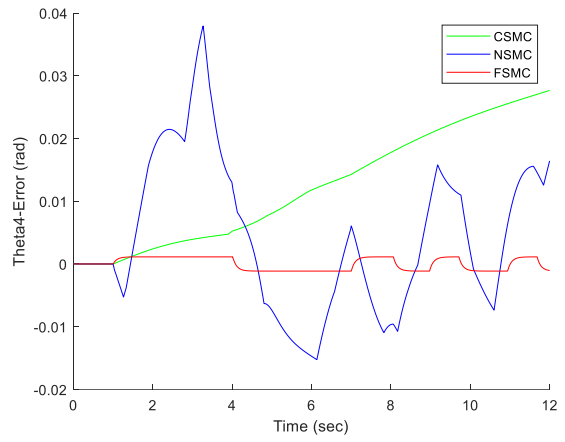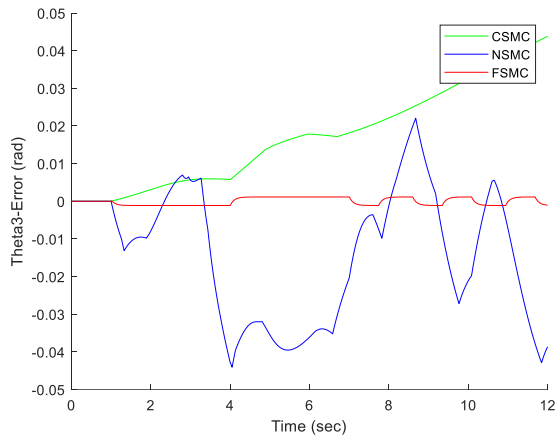
Figure *4*.5 Position tracking error of joints under CSMC, NSMC, and FSMC.
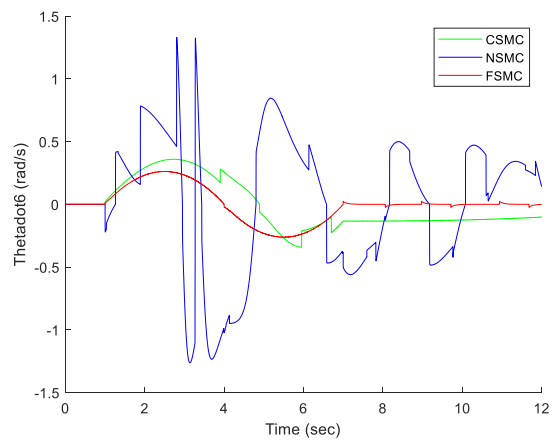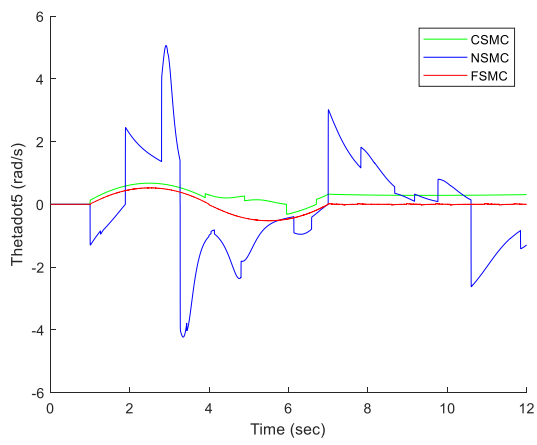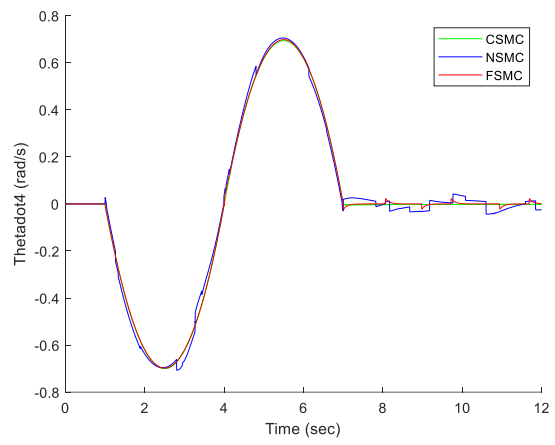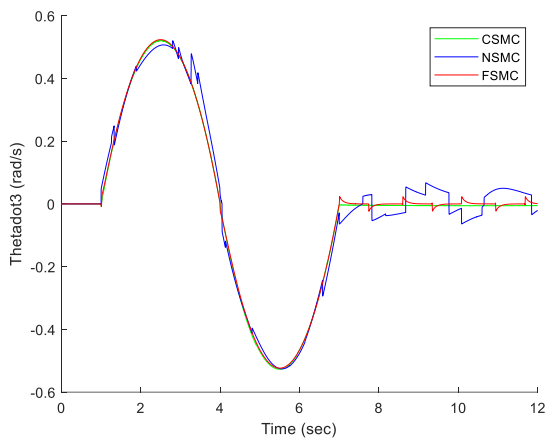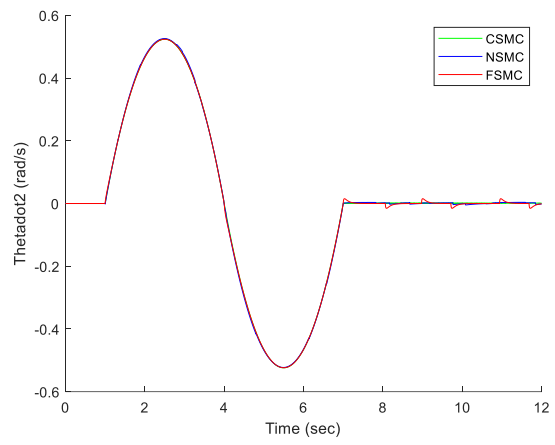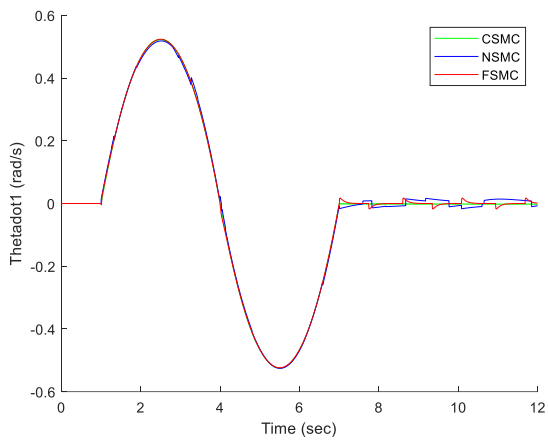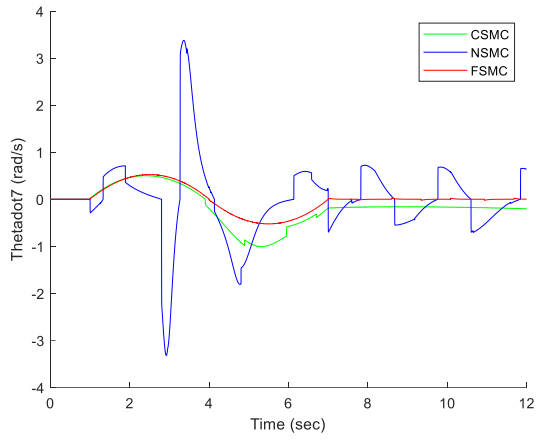
Figure *4*.6 Velocity of joints under CSMC, NSMC, and FSMC.
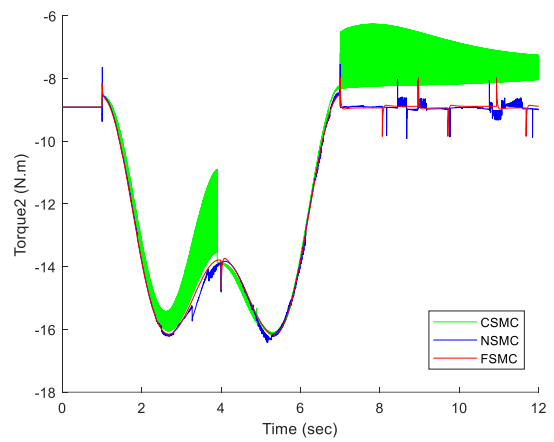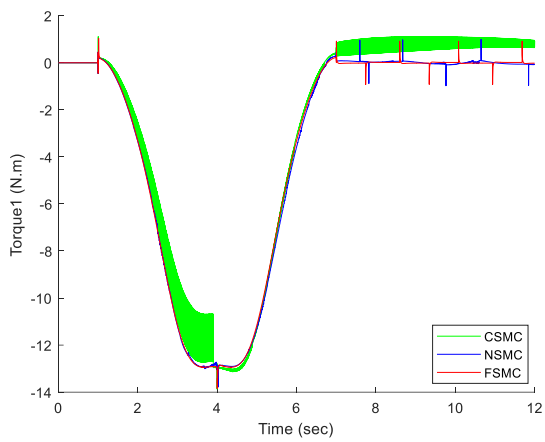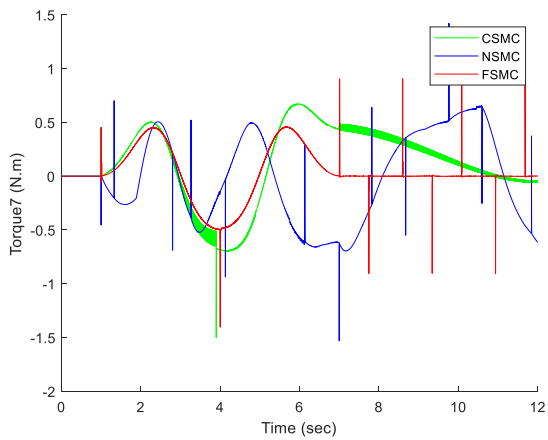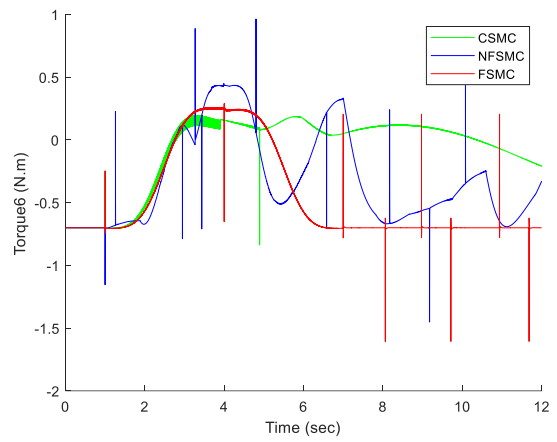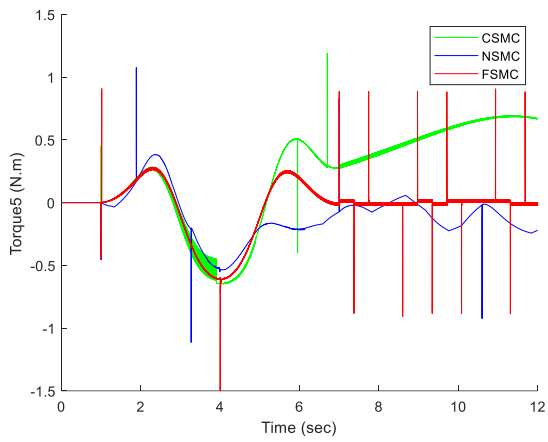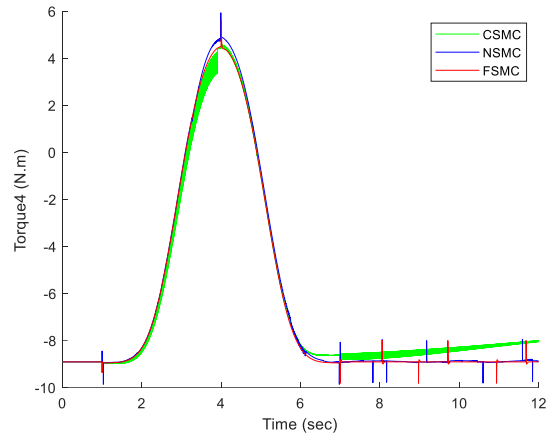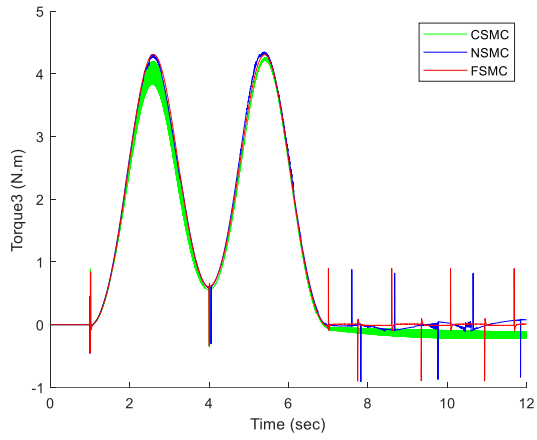
Figure *4.*7 Control effort using CSMC, NSMC, and FSMC.
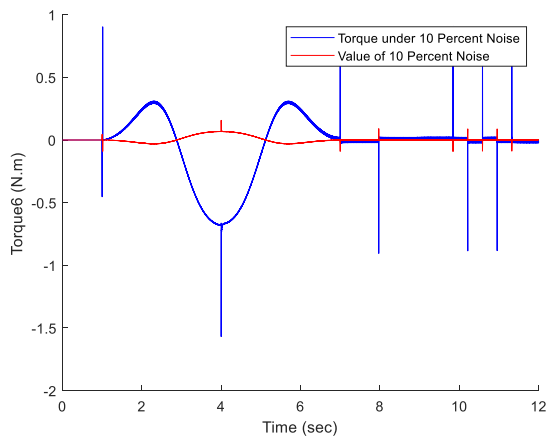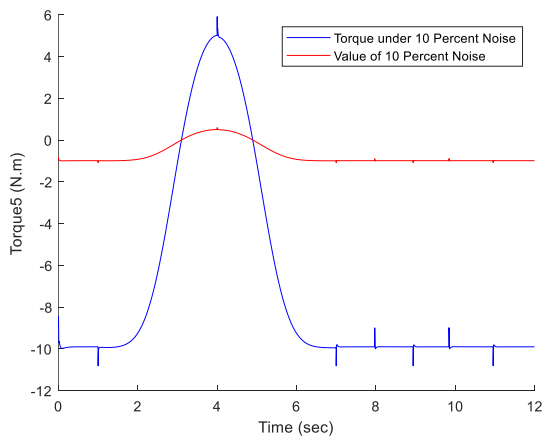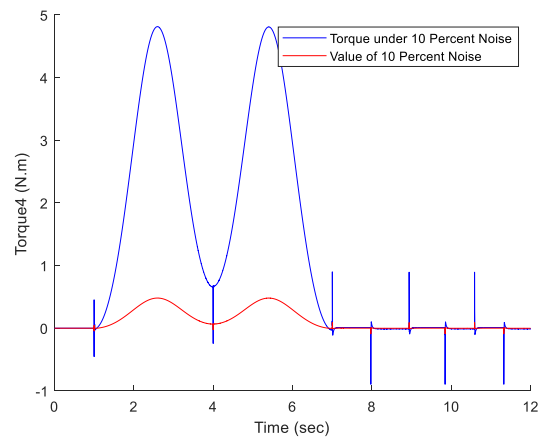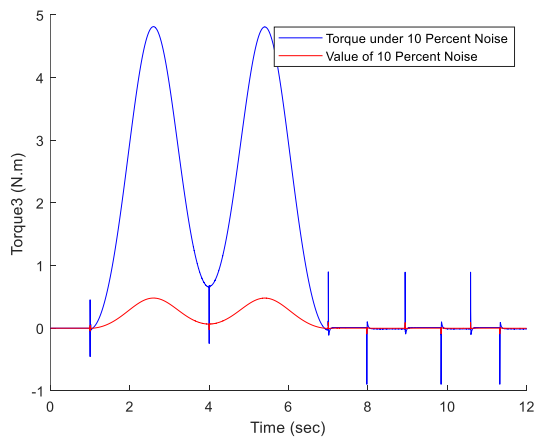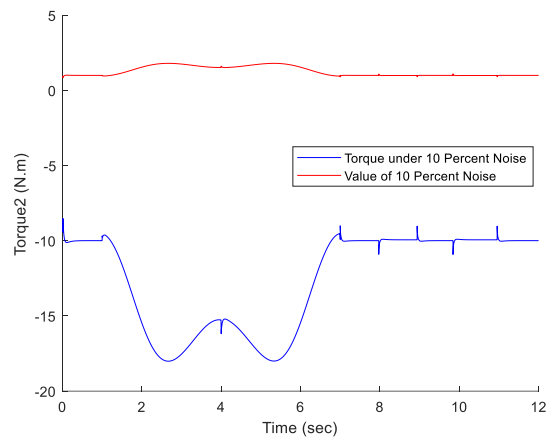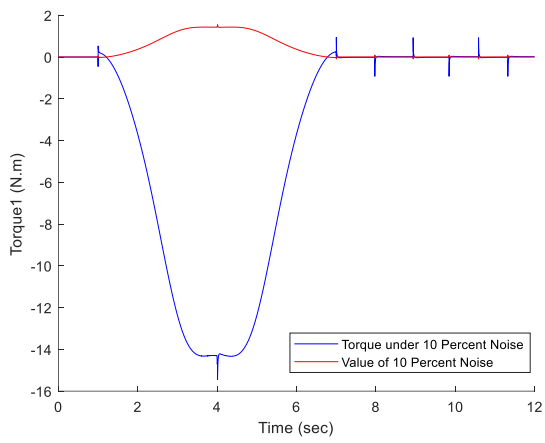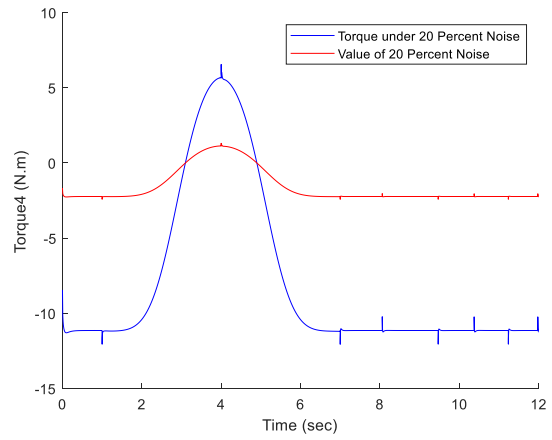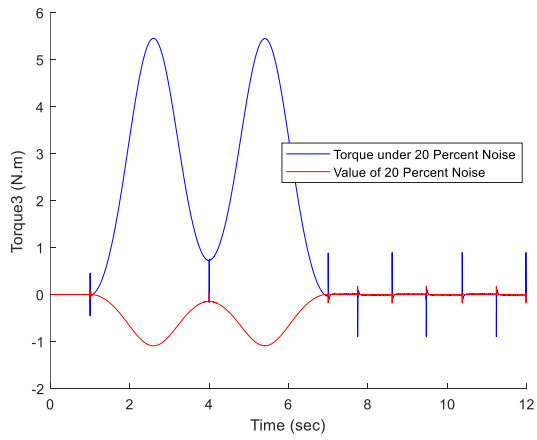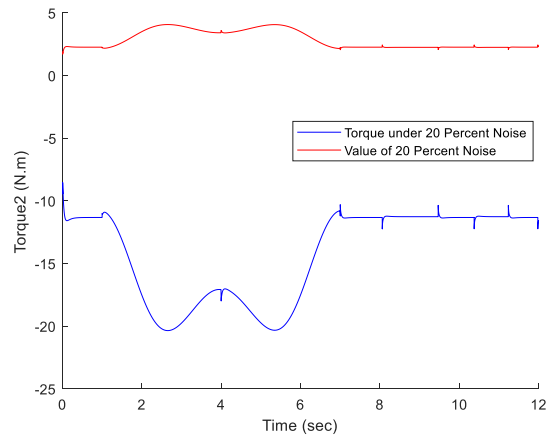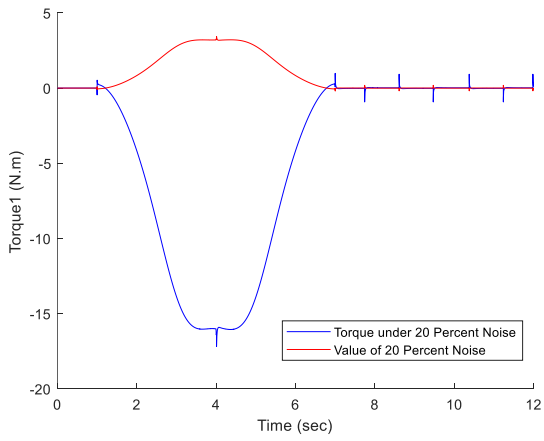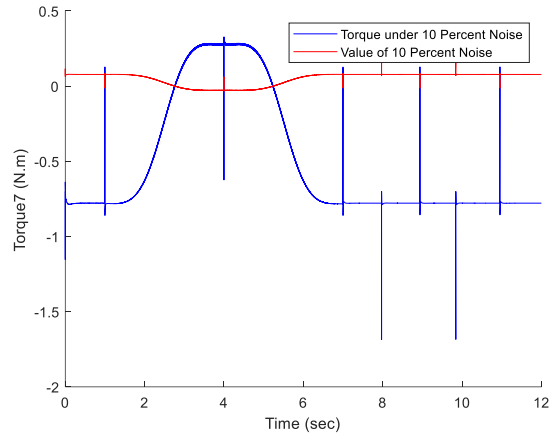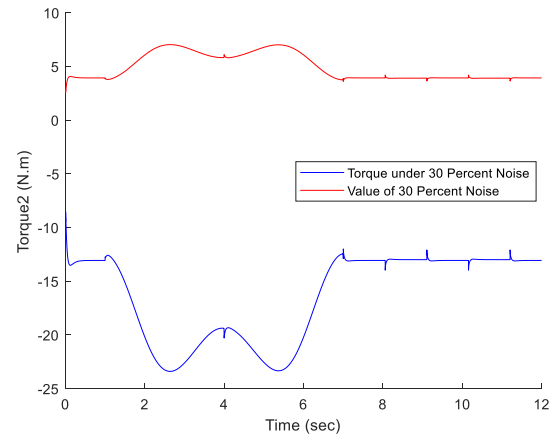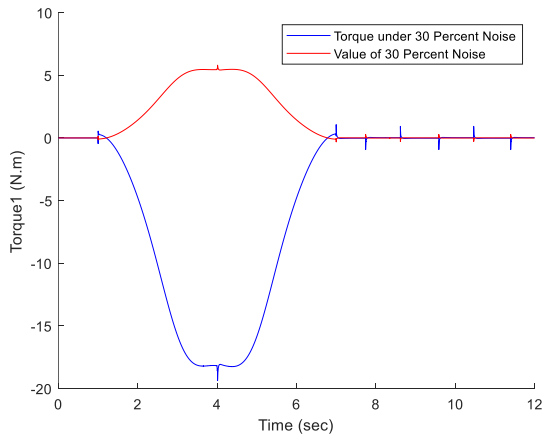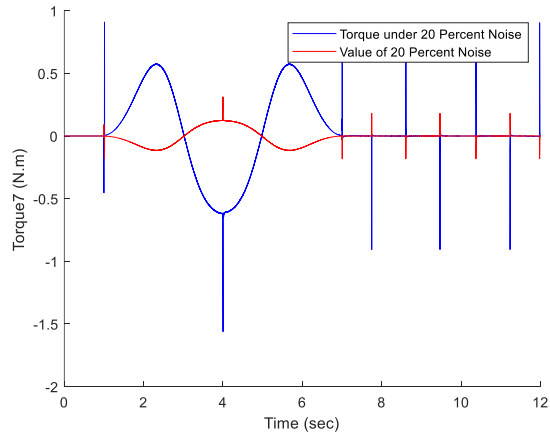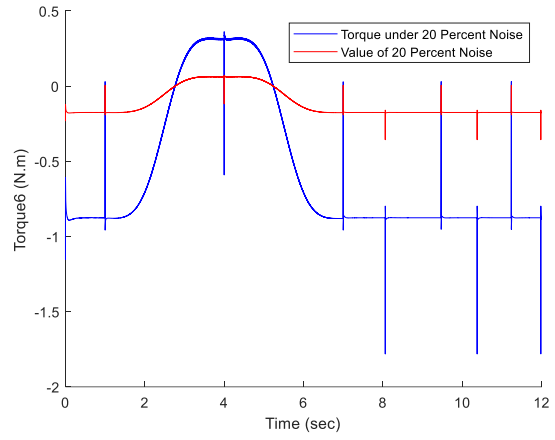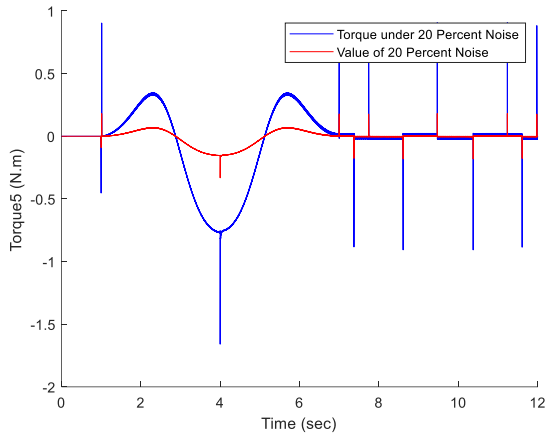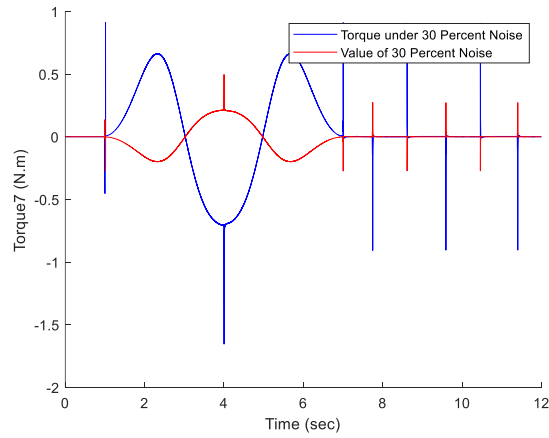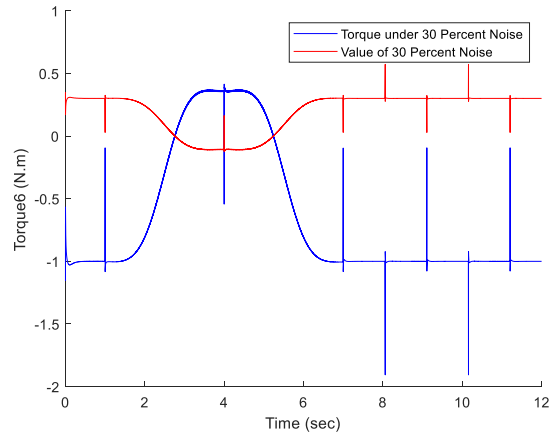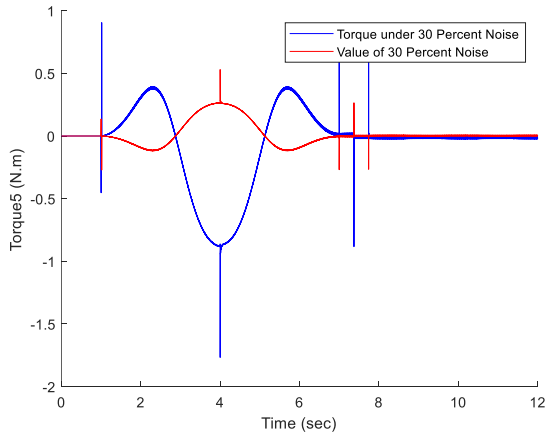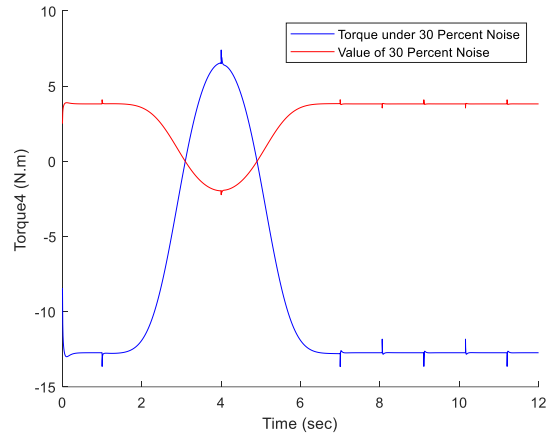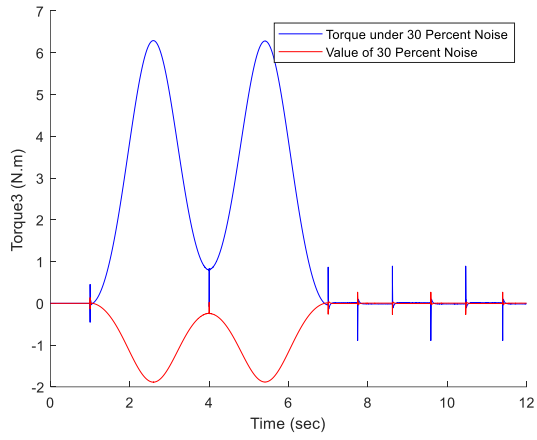
Figure *4.*8 Robustness verification of FSMC.

Figure 4.6 illustrates the joints velocities corresponding to the trajectories shown in Figure 4.4. Simulation results in Figure 4.5 demonstrated better trajectory tracking performance of FSMC compared to other controllers. To check the robustness of the FSMC, joint resistance to motion in the form of 10 percent of joint torque, 20 percent of joint torque, and 30 percent of joint torque are applied (Figure 4.8) to the exoskeleton robot. The simulation results are plotted in Figure 4.8, where it is observed that the FSMC can effectively overcome that artificially induced joint resistance.

4.4.2 A 2DoFs robot manipulator

Simulation Parameters:

For simulation, the robot structure (Figure 4.3) properties are chosen as L_1=320mm, L_2=360mm, m_1=386 gr, and m_2=722 gr.

The NSMC parameters are K_1=10000 and K_2=10000, and

The FSMC parameters are chosen as λ=100, α=15, and μ=0.5, and K_s =50

The control parameters are selected by trial and error to obtain suitable results.

When a robot encounters chattering, it makes the robot unstable.
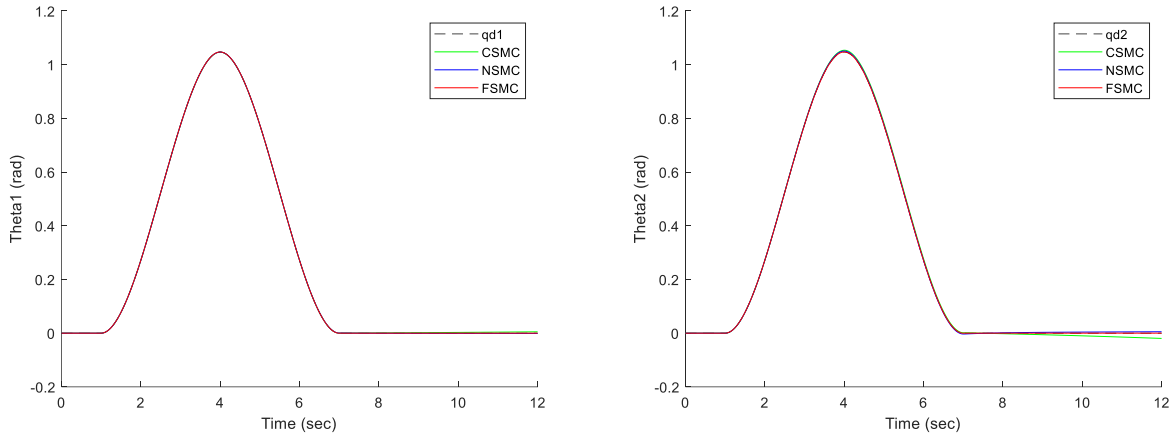
Figure *4.*9 Trajectory tracking of a 2DoFs robotic manipulator under CSMC, NSMC, and FSMC.

Figure 4.9 illustrates the trajectory tracking of the robot joints under CSMC, NSMC, and FSMC. The tracking errors of joints corresponding to the trajectories shown in Figure 4.9 are plotted in Figure 4.10. Figure 4.11 illustrates the joints velocities corresponding to the trajectories shown in Figure 4.9, whereas Figure 4.12 presents the control efforts. Simulation results in Figure 4.10 demonstrated better trajectory tracking performance of FSMC compared to other controllers. To check the robustness of the FSMC, joint resistance to motion in the form of 10 percent of joint torque, 20 percent of joint torque, and 30 percent of joint torque are applied (Figure 4.13) to the robot. The simulation results are plotted in Figure 4.13, where it is observed that the FSMC can effectively overcome that artificially induced joint resistance.
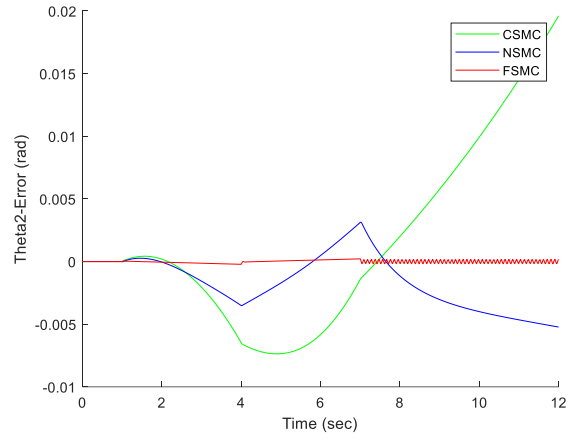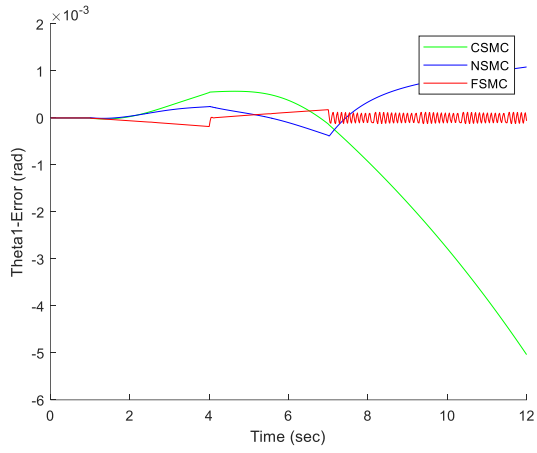
Figure *4.*10 Tracking error of joints under CSMC, NSMC and FSMC.
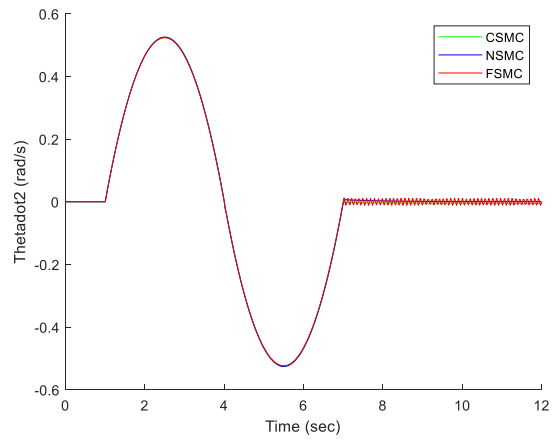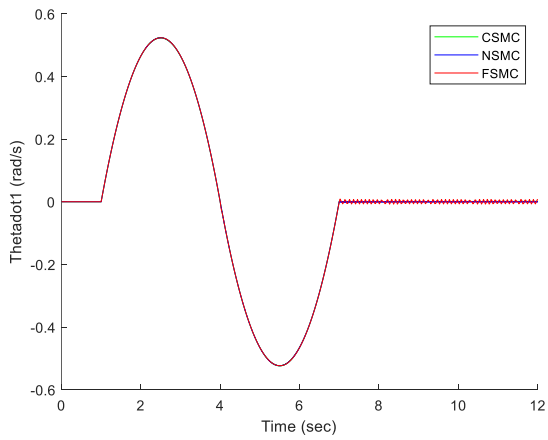
Figure *4.*11 Velocity of joints under CSMC, NSMC and FSMC.
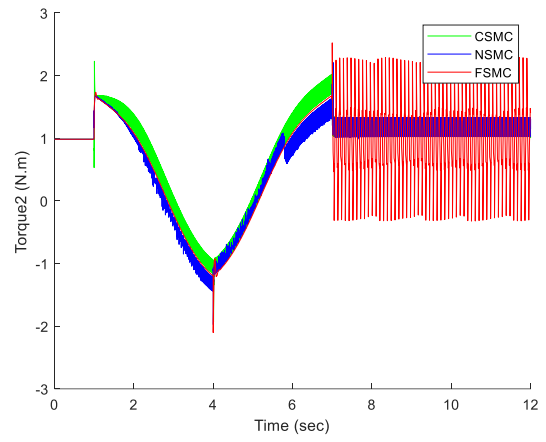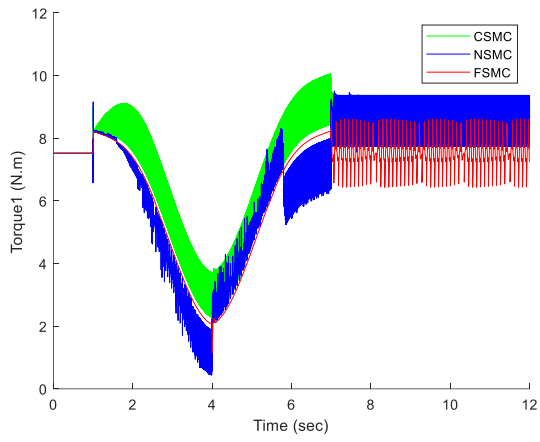
Figure 4.12 Control effort of CSMC, NSMC and FSMC.
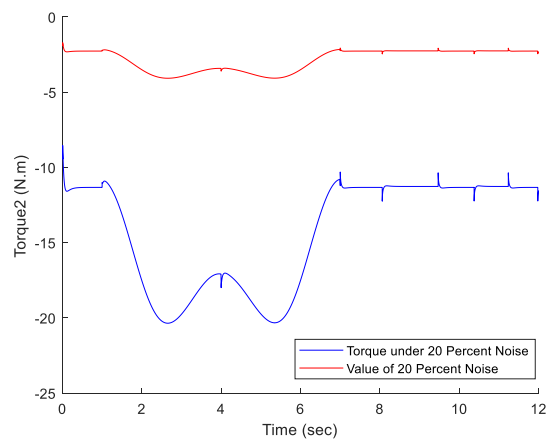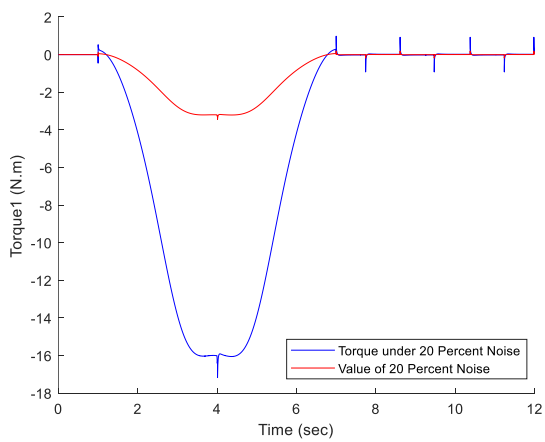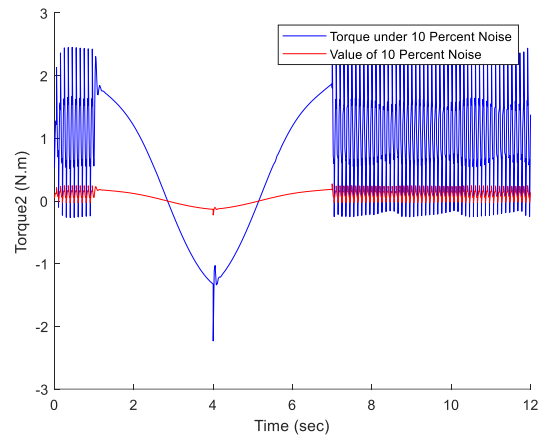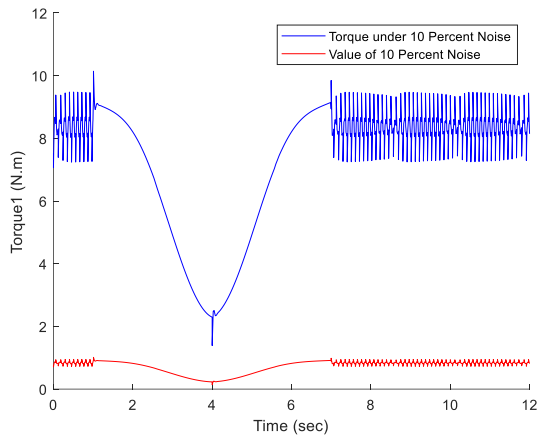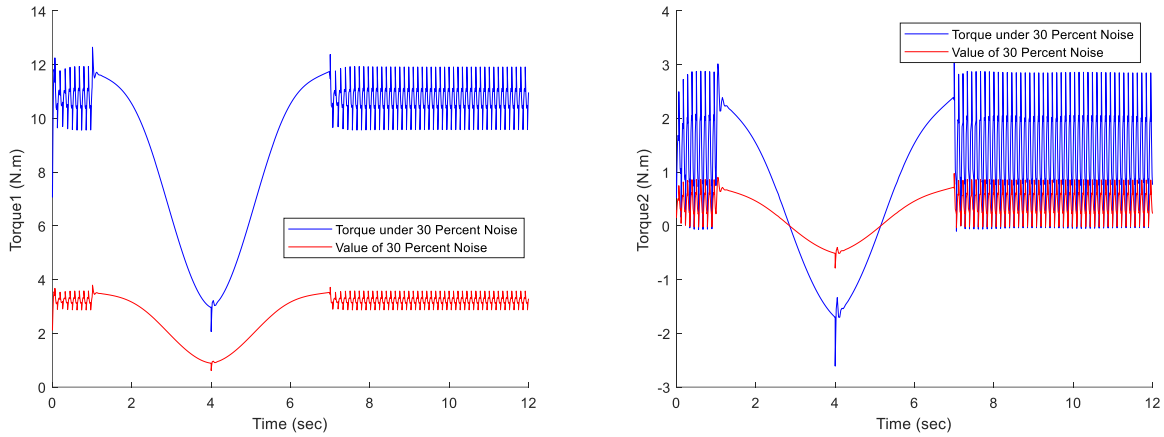
Figure *4*.13 Robustness verification of FSMC.

4.5 Experimental Results with New sliding mode control (NSMC).

In this research, only the proposed NSMC was implemented on a 2 DoFs robot manipulator..

4.5.1 Experimental Setup

The experimental setup used to implement the proposed NSMC on a 2 DoF robot manipulator is shown in Figure 4.14.
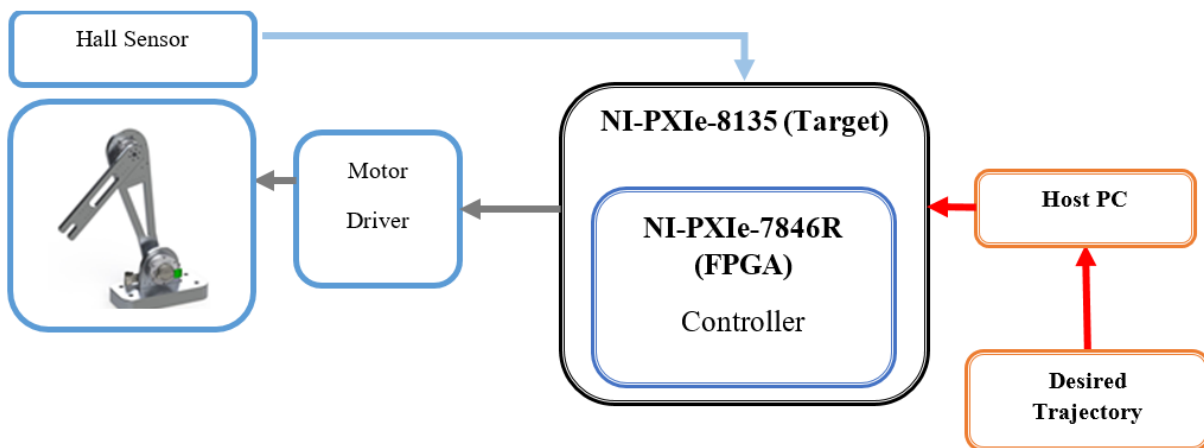
Figure *4*.14 Experimental setup

The 2DoFs robot used in this research was powered by two Maxon motors (EC45) integrated with

harmonic drive. Figure 4.15 illustrates the control architecture of the system. The proposed controller runs

in NI-PXIe (Figure 4.15, the sampling rate of 1.25 ms). As also seen in Figure 4.15, a low-level Proportional

Integral (PI) controller to control the desired current runs at 50μs (Figure 4.15) inside the FPGA.
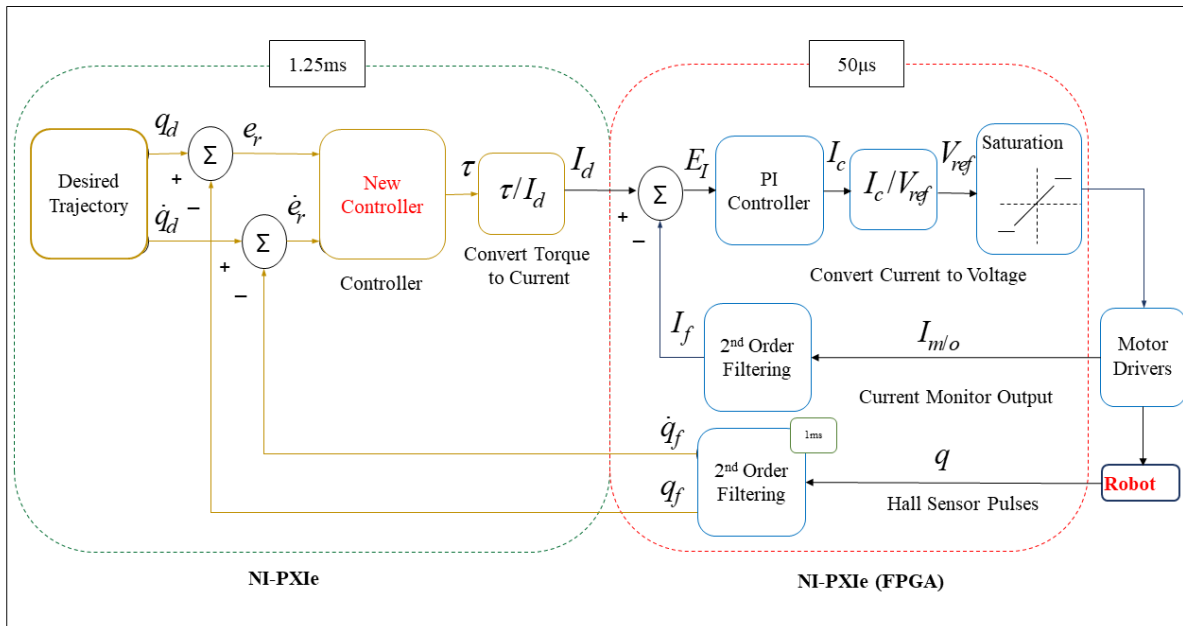
Figure *4.*15 Control architecture
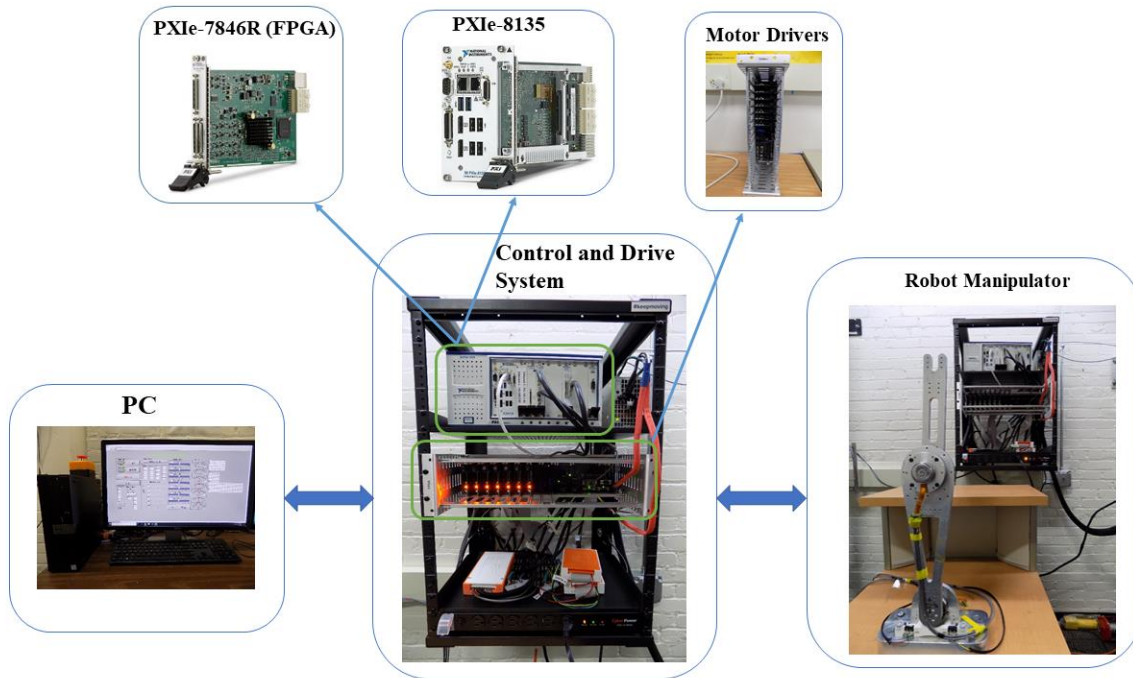
Figure *4*.16 Hardware of the 2 DoFs robot

The feedback current signals measured from the motor drivers (at a sampling rate a1ms) are also filtered with a second-order filter (sampling parameters: ζ=0.90, and ω_0=3000 rad/s) prior to being sent to the PI controller. Figure 4.16 shows the hardware of the 2 DoF robot.

4.5.2 Results

The robot structure properties are chosen as L_1=320mm, L_2=360mm, m_1=386 gr, and m_2=722 gr. The controller parameters are selected as $k_1 = diag\{580,580\}$, $k_2 = diag\{50,50\}$, $K_r = diag\{30,30\}$, $\mu_1 = diag\{40,40\}$, and $\mu_2 = diag\{40,40\}$.

Figure 4.17 shows the results of trajectory tracking under the CSMC and NSMC, and Figure 4.18 illustrates the corresponding tracking errors. It is evident from Fig. 4.18 that the proposed NSMC controller shows better tracking performance compared to CSMC. Figure 4.19 shows the control input signals under SMC and NSMC, where it is observed that NSMC exhibits no/very low chattering.
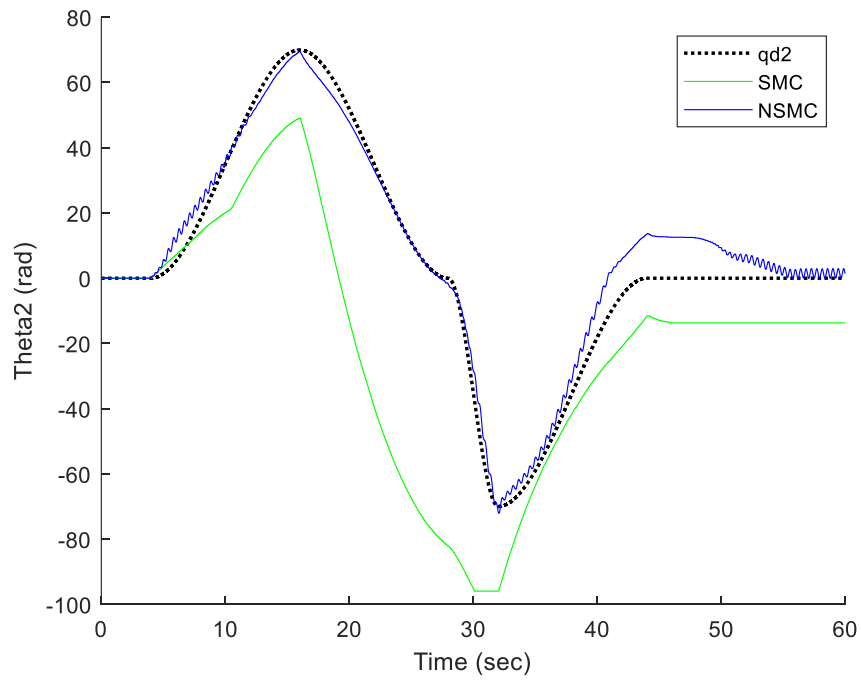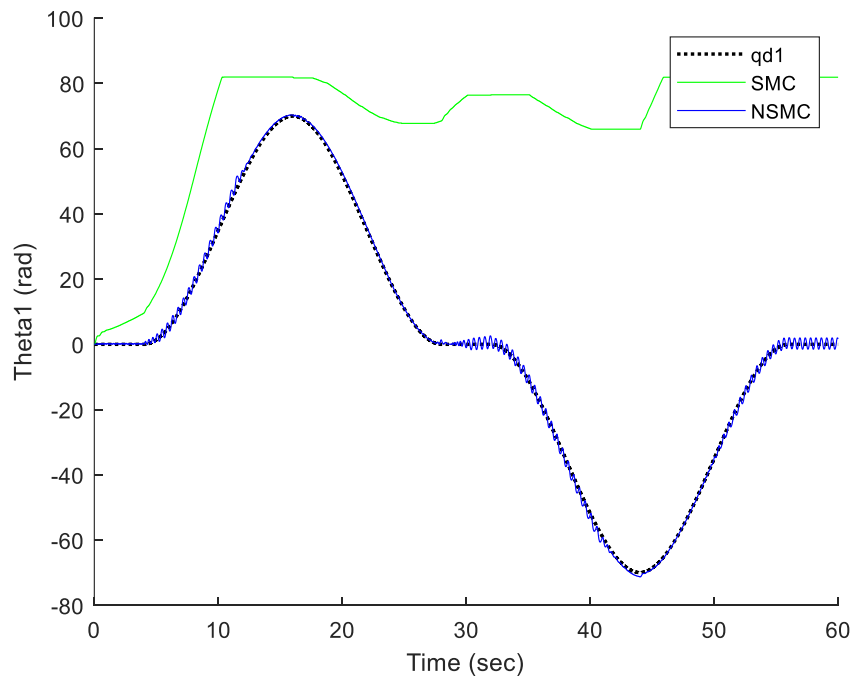
Figure *4*.17 Trajectory Tracking of a 2DoFs Robot under SMC and NSMC
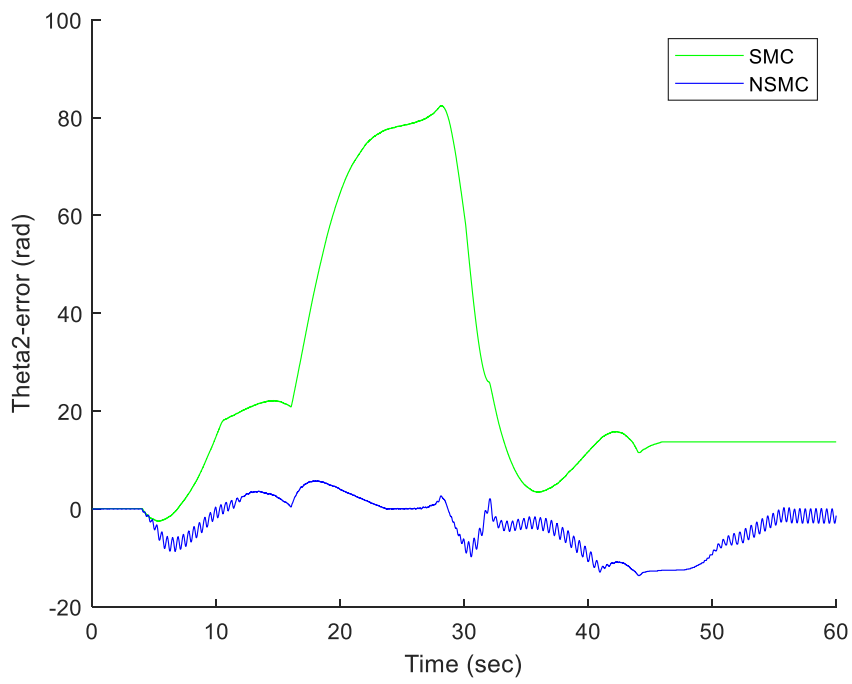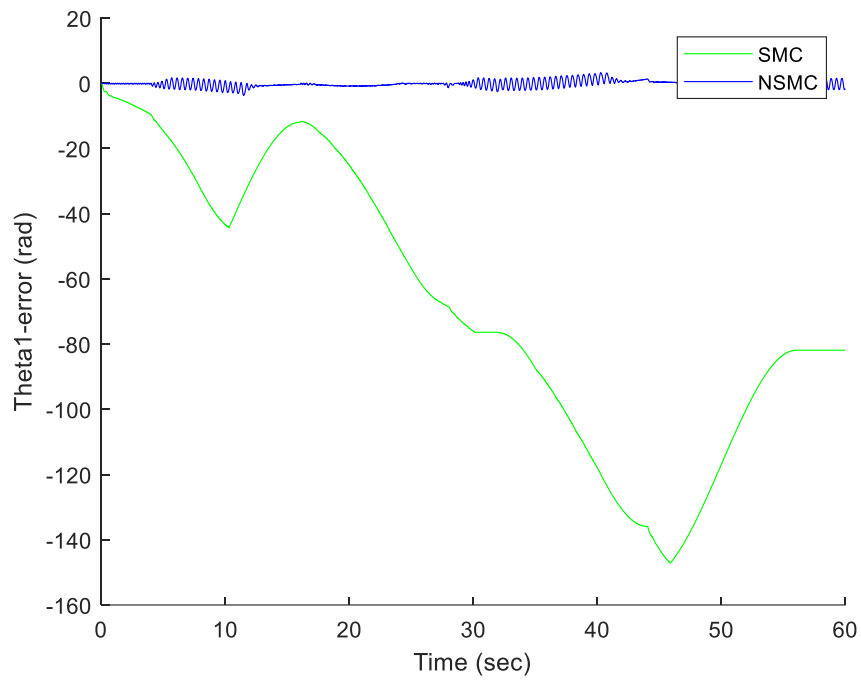
Figure *4*.18 Tracking error of joints under SMC, and NSMC.
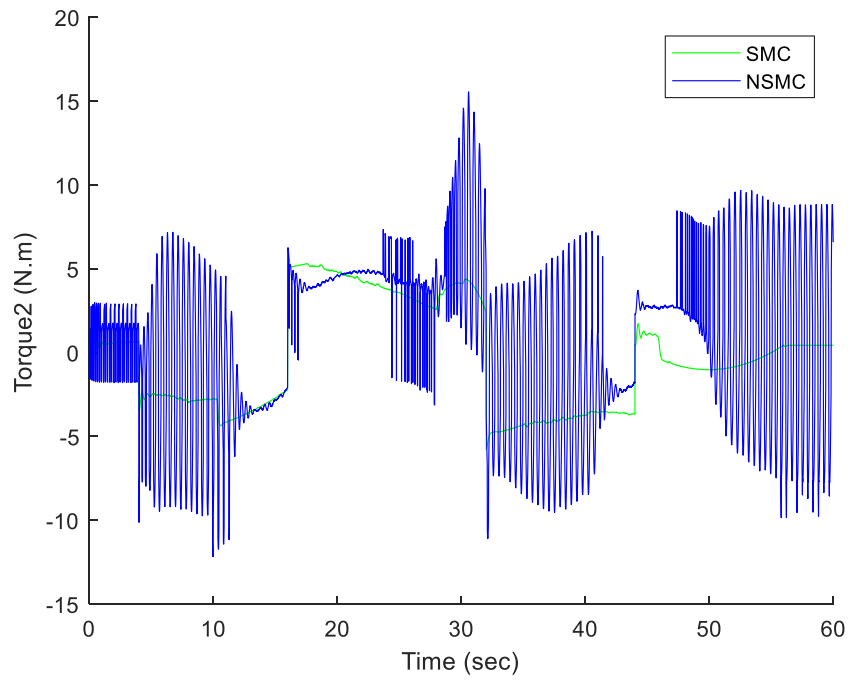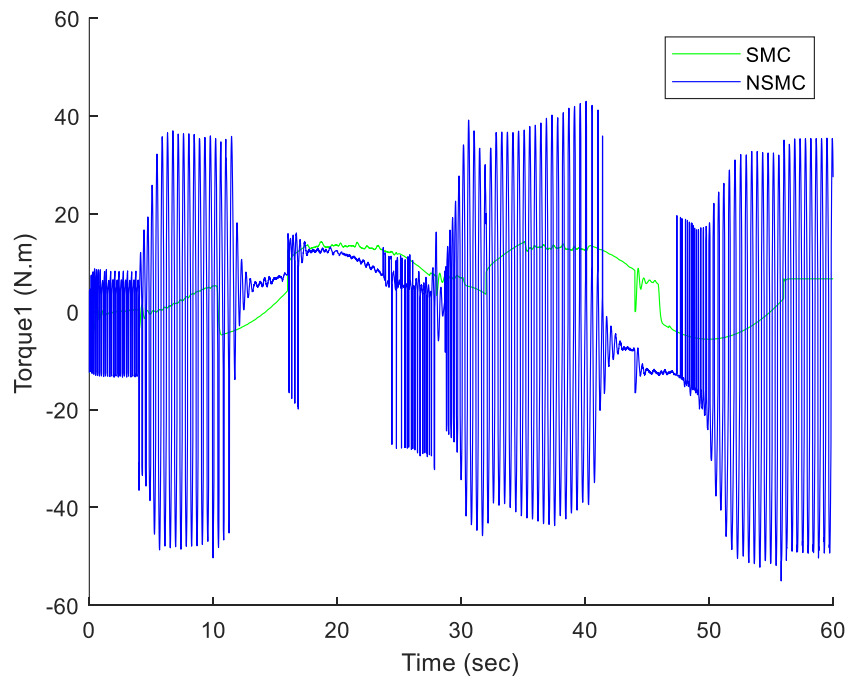
Figure *4*.19 Control input signals under SMC and NSMC.

Chapter 5

Conclusion and Future Works

5.1 Conclusion

This research proposed three robust nonlinear controllers based on sliding mode control to reduce chattering, improve robustness, decrease trajectory tracking error, and accelerate faster convergence. The results are summarized below:

- The proposed sliding mode controllers, namely robust sliding mode control, new sliding mode control, and fractional sliding mode control, were applied on three different dynamic systems that include a MEMS gyroscope, an Exoskeleton robot, and a 2DoFs robot manipulator.

- Simulation results demonstrated that fractional sliding mode control performance (i.e., finite-time convergence, robustness, chattering reduction, and dynamic trajectory tracking) was better than the conventional sliding mode control, robust sliding mode control, and new sliding mode control.

- In the dynamic simulation, to simulate the external disturbance, random noises were applied on the MEMS gyroscope, whereas 10% to 30% joint torques were applied on the exoskeleton robot and the 2 DoFs robot manipulator. The simulation was carried out with the proposed fractional sliding mode control. Results demonstrated that fractional sliding mode control is robust against external disturbances.

- The fractional sliding mode control shows the convergence of error to zero in finite time in all three dynamic systems. For instance, in the case of the 2 DoF robot manipulator, the error was wholly converged to zero after 2 sec under fractional sliding mode control.

- Simulation results evidence that the proposed fractional sliding mode control significantly reduced the chattering compared to the other three controllers.

- The experiment was conducted with the proposed NSMC on a 2DoFs robot manipulator. The results show better tracking performance of the NSMC compared with CSMC.

5.2 Future Works

The future research works include experimentation validation of all the proposed controllers on different dynamic systems that includes but are not limited to MEMS, exoskeleton robots, and other robotic manipulators in different operating conditions.

Appendix A

$$q = \begin{bmatrix} \theta_1 \\ \theta_2 \end{bmatrix}$$

$$M(q) = \begin{bmatrix} (M_1 + M_2)L_1^2 + M_2 L_2^2 + 2M_2 L_1 L_2 \cos\theta_2 & M_2 L_2^2 + M_2 L_1 L_2 \cos\theta_2 \\ M_2 L_2^2 + M_2 L_1 L_2 \cos\theta_2 & M_2 L_2^2 \end{bmatrix}$$

$$N(q, \dot{q}) = \begin{bmatrix} -M_2 L_1 L_2 \sin\theta_2 (2\dot{\theta}_1 \dot{\theta}_2 + \dot{\theta}_2^2) \\ -M_2 L_1 L_2 \sin\theta_2 \dot{\theta}_1 \dot{\theta}_2 \end{bmatrix}$$

$$G(q) = \begin{bmatrix} -(M_1 + M_2)g L_1 \sin\theta_1 - M_2 g L_2 \sin(\theta_1 + \theta_2) \\ -M_2 g L_2 \sin(\theta_1 + \theta_2) \end{bmatrix}$$

$$\tau = \begin{bmatrix} \tau_1 \\ \tau_2 \end{bmatrix}$$

Appendix B
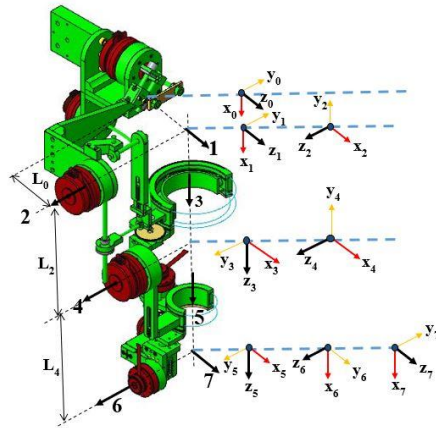
Figure 5.1 Reference frames of exoskeleton robot [68].

Masses of links

```
m1=5.440530749; m2 = 3.681985727; m3=3.453863929; m4 = 1.248221;
m5=1.349766; m6=1.085; m7 = 0.22;
```

Link length

```
% Mechanisms Fixed Parameter
th11=deg2rad(-45);    % Fixed angle
th21=deg2rad(180);    % Fixed angle
L12=70/1000;    % in meter
L21=40/1000; L22 =220.388/1000; % in meter, From CAD

L0=231.35/1000;
L34=82.0452/1000;      % Fixed Length between Cuff position and Elbow axis
L4=297.928/1000;   L7=62.3626/1000;
```

Center of Gravity

```
Pc11=1e-3*[-2.5239911e+01; -1.5121379e+02; -1.6240684e+02];
Pc22=1e-3*[-3.4802404e-01; -1.5549869e+02;  1.8189489e+02];
Pc33=1e-3*[-1.4635716e+00;  1.4629969e+02; -2.1562809e+01];
Pc44=1e-3*[-5.7671125e+01; -1.4231862e+02;  4.0644131e+01];
Pc55=1e-3*[-1.8162879e+01;  8.3354291e+01; -4.8300119e+01];
Pc66=1e-3*[-5.5555846e-01; -9.2656899e+01;  3.3806189e+01];
Pc77=1e-3*[2.3881007e+01;  0.0000000e+00; -8.0984229e+01];
```

Inertia tensor

$Ixx1 = 1.5821554e+07;$ $Ixy1 = 2.8977925e+05;$ $Ixz1 = -2.9103717e+05;$
$Iyy1 = 3.1418801e+06;$ $Iyz1 = 5.2110805e+06;$
$Izz1 = 1.3149358e+07;$

$Ixx2 = 5.4133526e+04;$ $Ixy2 = 2.2552398e+01;$ $Ixz2 = -1.0498490e+02;$
$Iyy2 = 3.0720402e+04;$ $Iyz2 = -1.1115691e+03;$
$Izz2 = 3.2736876e+04;$

$Ixx3 = 2.1468619e+04;$ $Ixy3 = -9.0220381e+01;$ $Ixz3 = 5.5602768e+00;$
$Iyy3 = 1.0830093e+04;$ $Iyz3 = -7.5909494e+03;$
$Izz3 = 1.9790383e+04;$

$Ixx4 = 6.5326368e+03;$ $Ixy4 = -9.5450564e+02;$ $Ixz4 = -1.9750886e+03;$
$Iyy4 = 5.6739686e+03;$ $Iyz4 = -1.9814171e+03;$
$Izz4 = 5.4579768e+03;$

$Ixx5 = 9.3746570e+03;$ $Ixy5 = -2.0632768e+03;$ $Ixz5 = -1.3410291e+03;$
$Iyy5 = 5.0513403e+03;$ $Iyz5 = -3.9763402e+03;$
$Izz5 = 7.6482132e+03;$

$Ixx6 = 4.5491237e+03;$ $Ixy6 = 4.7853672e+00;$ $Ixz6 = -1.7819407e+01;$
$Iyy6 = 2.9356115e+03;$ $Iyz6 = -1.7606246e+03;$
$Izz6 = 2.2434622e+03;$

$Ixx7 = 6.8343705e+01;$ $Ixy7 = 0;$ $Ixz7 = -5.0030031e+01;$
$Iyy7 = 3.0672986e+02;$ $Iyz7 = 0;$
$Izz7 = 3.0717512e+02;$

Bibliography

[1]   Athans, M. (1971). On the LQG problem. IEEE Transactions on Automatic Control, 16(6), 528-528.

[2]   Utkin, V. I. (1993). Sliding mode control design principles and applications to electric drives. IEEE transactions on industrial electronics, 40(1), 23-36.

[3]   Utkin, V., & Lee, H. (2006, June). Chattering problem in sliding mode control systems. In *International Workshop on Variable Structure Systems, 2006. VSS'06.* (pp. 346-350). IEEE.

[4]   Kachroo, P., & Tomizuka, M. (1996). Chattering reduction and error convergence in the sliding-mode control of a class of nonlinear systems. IEEE Transactions on Automatic Control, 41(7), 1063-1068.

[5]   Wang X, Xu X. B, Zhang D. W, Wu X. Z: Pre-buried mask wet etching for suspended silicon microstructures applied in rocking mass micro-gyroscope. Microsystem Technologies (2017).

[6]   Saxena S, Sharma R, Pant B. D: Design and development of guided four beam cantilever type MEMS based piezoelectric energy harvester. Microsystem Technologies, 23(6), 1751-1759 (2017)

[7]   Rahmani M, Ghanbari A, Ettefagh M. M: Hybrid neural network fraction integral terminal sliding mode control of an Inchworm robot manipulator. Mechanical Systems and Signal Processing, 80, 117-136 (2016)

[8]   Rahmani M, Ghanbari A, Ettefagh M. M: Robust adaptive control of a bio-inspired robot manipulator using bat algorithm. Expert Systems with Applications, 56, 164-176 (2016)

[9]   Rahmani, M, Ghanbari A, Ettefagh M. M: A novel adaptive neural network integral sliding-mode control of a biped robot using bat algorithm. Journal of Vibration and Control, 1077546316676734 (2016)

[10]   Batur C, Sreeramreddy T, Khasawneh Q: Sliding mode control of a simulated MEMS gyroscope. ISA transactions, 45(1), 99-108 (2006)

[11]   Fei J, Yuan Z: Dynamic sliding mode control of MEMS gyroscope. In Control Applications (CCA), 2013 IEEE International Conference on (pp. 437-442). IEEE (2013)

[12]   Utkin, V., & Lee, H. (2006, June). Chattering problem in sliding mode control systems. In International Workshop on Variable Structure Systems, 2006. VSS'06. (pp. 346-350). IEEE.

[13]   Chu Y, Fei J: Adaptive global sliding mode control for MEMS gyroscope using RBF neural network. Mathematical Problems in Engineering, (2015)

[14]   Ren J, Zhang R, Xu B: Adaptive fuzzy sliding mode control of MEMS gyroscope with finite time convergence. Journal of Sensors, (2016)

[15]   Wang S, Fei J: Robust adaptive sliding mode control of MEMS gyroscope using T–S fuzzy model. Nonlinear Dynamics, 77(1-2), 361-371 (2014)

[16]   Xin M, Fei J: Adaptive vibration control for MEMS vibratory gyroscope using

backstepping sliding mode control. Journal of Vibration and Control, 21(4), 808-817 (2015)

[17]   Fei J, Yan W, Yang Y: Adaptive nonsingular terminal sliding mode control of MEMS gyroscope based on backstepping design. International Journal of Adaptive Control and Signal Processing, 29(9), 1099-1115 (2015)

[18]   Ghanbari A, Moghanni-Bavil-Olyaei M. R: Adaptive fuzzy terminal sliding-mode control of MEMS z-axis gyroscope with extended Kalman filter observer. Systems Science & Control Engineering: An Open Access Journal, 2(1), 183-191 (2014)

[19]   Fei J, Yang Y: Robust neural network control of MEMS gyroscope using adaptive sliding mode compensator. Robotica, 34(3), 497-512 (2016)

[20]   Asad Y. P, Shamsi A, Tavoosi J.: Backstepping-Based Recurrent Type-2 Fuzzy Sliding Mode Control for MIMO Systems (MEMS Triaxial Gyroscope Case Study). International Journal of Uncertainty, Fuzziness and Knowledge-Based Systems, 25(02), 213-233 (2017)

[21]   Chu Y, Fang Y, Fei J:Adaptive neural dynamic global PID sliding mode control for MEMS gyroscope. International Journal of Machine Learning and Cybernetics, 8(5), 1707-1718 (2017)

[22]   Rahmani M: MEMS gyroscope control using a novel compound robust control. ISA Transactions, https: //doi.org/10.1016/j.isatra.2017.11.009i (2017)

[23]   L. Wu, Y. Gao, J. Liu, and H. Li, "Event-triggered sliding mode control of stochastic

systems via output feedback," Automatica, vol. 82, pp. 79-92, Aug 2017.

[24] J. Liu, H. An, Y. Gao, C. Wang, and L. Wu, "Adaptive control of hypersonic flight vehicles with limited angle-of-attack," IEEE/ASME Transactions on Mechatronics, vol. 23, pp. 883-94, Apr 2018.

[25] J. Liu, Y. Yin, W. Luo, S. Vazquez, L. G. Franquelo, and L. Wu, "Sliding mode control of a three-phase AC/DC voltage source converter under unknown load conditions: Industry applications," IEEE Transactions on Systems, Man, and Cybernetics: Systems, vol. 99, pp. 1-0, Dec 2017.

[26] J. Liu, Y. Gao, X. Su, M. Wack, and L. Wu. Disturbance-observer-based control for air management of PEM fuel cell systems via sliding mode technique. IEEE Transactions on Control Systems Technology. 2018 Feb 21(99):1-0.

[27] J. Li and Q. Zhang, "A linear switching function approach to sliding mode control and observation of descriptor systems," Automatica, vol. 95, pp. 112-21, Sep 2018.

[28] S. Zhu, X. Jin, B. Yao, Q. Chen, X. Pei, and Z. Pan, "Nonlinear sliding mode control of the lower extremity exoskeleton based on human–robot cooperation," International Journal of Advanced Robotic Systems, Vol. 13, pp. 1729881416662788, Oct 2016.

[29] Y. Long, Z. J. Du, W. D. Wang, and W. Dong, "Robust sliding mode control based on GA optimization and CMAC compensation for lower limb exoskeleton," Applied bionics and biomechanics, 2016.

[30] Z. Wang, S. Zhu, Q. Chen, X. Zhang, and Y. Song, "Sliding mode control of electro-

hydraulic servo system for lower-limb exoskeleton based on RBF neural network," In2015 IEEE 10th Conference on Industrial Electronics and Applications (ICIEA), pp. 79-83, Jun 2015.

[31]   M. Babaiasl, S. N. Goldar, M. H. Barhaghtalab, and V. Meigoli, "Sliding mode control of an exoskeleton robot for use in upper-limb rehabilitation," In2015 3rd RSI International Conference on Robotics and Mechatronics (ICROM), pp. 694-701, Oct 2015.

[32]   B. O. Mushage, J. C. Chedjou, and Kyamakya K, "Fuzzy neural network and observer-based fault-tolerant adaptive nonlinear control of uncertain 5-DOF upper-limb exoskeleton robot for passive rehabilitation," Nonlinear Dynamics, vol. 87, pp. 2021-37, Feb 2017.

[33]   S. Ahmed, H. Wang, and Y. Tian, "Model-free control using time delay estimation and fractional-order nonsingular fast terminal sliding mode for uncertain lower-limb exoskeleton," Journal of Vibration and Control, vol. 24, pp. 5273-90, Nov 2018.

[34]   H. Su, Z. Li, G. Li, and C. Yang, "EMG-Based neural network control of an upper-limb power-assist exoskeleton robot," International Symposium on Neural Networks, pp. 204-211, Springer, Berlin, Heidelberg, July 2013.

[35]   B. Achili, T. Madani, B. Daachi, and K. Djouani, "Adaptive observer based on MLPNN and sliding mode for wearable robots: Application to an active joint orthosis," Neurocomputing, vol. 197, pp. 69-77, Jul 2016.

[36]   S. Han, H. Wang, and Y. Tian, "Model-free based adaptive nonsingular fast terminal sliding mode control with time-delay estimation for a 12 DOF multi-functional lower limb exoskeleton," Advances in Engineering Software, vol. 119, pp. 38-47, May 2018.

[37]   T. Madani, B. Daachi, and K. Djouani, "Finite-time control of an actuated orthosis using fast terminal sliding mode," IFAC proceedings volumes, vol. 47, pp. 4607-12, Jan 2014.

[38]   S. Mefoued, "A robust adaptive neural control scheme to drive an actuated orthosis for assistance of knee movements," Neurocomputing, vol. 140, pp. 27-40, Sep 2014.

[39]   M. H. Rahman, M. Saad, J. P. Kenné, and P. S. Archambault, "Control of an exoskeleton robot arm with sliding mode exponential reaching law," International Journal of Control, Automation and Systems, vol. 11, pp. 92-104, Feb 2013.

[40]   B. Brahmi, M. Saad, M. H. Rahman, and C. Ochoa-Luna, "Cartesian trajectory tracking of a 7-DOF exoskeleton robot based on human inverse kinematics," IEEE Transactions on Systems, Man, and Cybernetics: Systems, vol. 18, pp. 1-2, May 2017.

[41]   Rathore, N., Fulwani, D., & Rathore, A. K. (2020). Event-triggered Sliding Mode Control for light load efficiency improvement in Power Converters. Control Engineering Practice, 100, 104429.

[42]   Rinaldi, G., & Ferrara, A. (2020). Automatic identification of the relative degree of nonlinear systems: Application to sliding mode control design and experimental assessment. Control Engineering Practice, 94, 104207.

[43]   Shtessel, Y., Fridman, L., & Plestan, F. (2016). Adaptive sliding mode control and

observation. International Journal of Control, 89(9), 1743-1746.

[44]   Falcón, R., Ríos, H., & Dzul, A. (2019). Comparative analysis of continuous sliding-modes control strategies for quad-rotor robust tracking. Control Engineering Practice, 90, 241-256.

[45]   Gracia, L., Solanes, J. E., Munoz-Benavent, P., Esparza, A., Miro, J. V., & Tornero, J. (2018). Cooperative transport tasks with robots using adaptive non-conventional sliding mode control. Control Engineering Practice, 78, 35-55.

[46]   Liaw, H. C., Shirinzadeh, B., & Smith, J. (2008). Sliding-mode enhanced adaptive motion tracking control of piezoelectric actuation systems for micro/nano manipulation. IEEE Transactions on Control Systems Technology, 16(4), 826-833.

[47]   Xiong, Y., Gao, Y., Yang, L., & Wu, L. (2019). An integral sliding mode approach to distributed control of coupled networks with measurement Quantization. Systems & Control Letters, 133, 104557.

[48]   Herrera, M., Camacho, O., Leiva, H., & Smith, C. (2020). An approach of dynamic sliding mode control for chemical processes. Journal of Process Control, 85, 112-120.

[49]   Yu, S., Xie, M., Wu, H., Ma, J., Li, Y., & Gu, H. (2020). Composite proportional-integral sliding mode control with feedforward control for cell puncture mechanism with piezoelectric actuation. ISA transactions.

[50]   Wang, X., van Kampen, E. J., & Chu, Q. (2019). Quadrotor fault-tolerant incremental nonsingular terminal sliding mode control. Aerospace Science and Technology, 95,

105514.

[51]   Wu, Y., Yu, X., & Man, Z. (1998). Terminal sliding mode control design for uncertain dynamic systems. *Systems & Control Letters*, *34*(5), 281-287.

[52]   Li, M., Liu, M., & Zhang, Y. (2020). Asynchronous adaptive dynamic output feedback sliding mode control for singular markovian jump systems with actuator faults and uncertain transition rates. Applied Mathematics and Computation, 371, 124958.

[53]   Zheng, K., Hu, Y., & Wu, B. (2020). Intelligent fuzzy sliding mode control for complex robot system with disturbances. European Journal of Control, 51, 95-109.

[54]   Jing, C., Xu, H., & Niu, X. (2019). Adaptive sliding mode disturbance rejection control with prescribed performance for robotic manipulators. ISA transactions, 91, 41-51.

[55]   Ferrara, A., Incremona, G. P., & Sangiovanni, B. (2019). Tracking control via switched Integral Sliding Mode with application to robot manipulators. Control Engineering Practice, 90, 257-266.

[56]   Yi, S., & Zhai, J. (2019). Adaptive second-order fast nonsingular terminal sliding mode control for robotic manipulators. ISA transactions, 90, 41-51.

[57]   Xia, Y., Fu, M., Shi, P., & Wang, M. (2010). Robust sliding mode control for uncertain discrete-time systems with time delay. IET Control Theory & Applications, 4(4), 613-624.

[58]   Zhang, Y., & Yan, P. (2019). Adaptive observer-based integral sliding mode control of a piezoelectric nano-manipulator. IET Control Theory & Applications, 13(14), 2173-

2180.

[59]   Che, Z., Yu, H., Yang, C., & Zhou, L. (2019). Passivity analysis and disturbance observer-based adaptive integral sliding mode control for uncertain singularly perturbed systems with input nonlinearity. IET Control Theory & Applications, 13(18), 3174-3183.

[60]   Erenturk, K. (2008). Nonlinear two-mass system control with sliding-mode and optimised proportional–integral derivative controller combined with a grey estimator. IET Control Theory & Applications, 2(7), 635-642.

[61]   Jie, W., Kim, H. H., Dad, K., & Lee, M. C. (2018). Terminal Sliding Mode Control with Sliding Perturbation Observer for a Hydraulic Robot Manipulator. IFAC-PapersOnLine, 51(22), 7-12.

[62]   Rathore, N., Fulwani, D., & Rathore, A. K. (2020). Event-triggered Sliding Mode Control for light load efficiency improvement in Power Converters. Control Engineering Practice, 100, 104429.

[63]   Yan W, Hou S, Fang Y and Fei J: Robust adaptive nonsingular terminal sliding mode control of MEMS gyroscope using fuzzy-neural-network compensator. International Journal of Machine Learning and Cybernetics,1-13 (2016)

[64]   Rahmani, M. (2018). MEMS gyroscope control using a novel compound robust control. ISA transactions, 72, 37-43.

[65]   Rahmani, M., & Rahman, M. H. (2019). An upper-limb exoskeleton robot control using

a novel fast fuzzy sliding mode control. Journal of Intelligent & Fuzzy Systems, 36(3), 2581-2592.

[66]   Eray, O., & Tokat, S. (2020). The design of a fractional-order sliding mode controller with a time-varying sliding surface. *Transactions of the Institute of Measurement and Control*, *42*(16), 3196-3215.

[67]   Jin, L., Gao, Q., Hou, Y., Sun, Z., Jia, L., & Li, K. (2015, December). Fractional neural sliding mode control for the electro-hydraulic servo system. In 2015 IEEE Advanced Information Technology, Electronic and Automation Control Conference (IAEAC) (pp. 810-815). IEEE.

[68]   Islam, M. R., Rahmani, M., & Rahman, M. H. (2020). A novel exoskeleton with fractional sliding mode control for upper limb rehabilitation. *Robotica*, *38*(11), 2099-2120.

[69]   C. L. Ochoa, M. H. Rahman, M. Saad, P. S. Archambault, and S. F. Bruce, "Admittance-based upper limb robotic active and active-assistive movements," International Journal of Advanced Robotic Systems, vol. 12, pp. 117, Sep 2015.

[70]   M. H. Rahman, OC. L. choa, M. J. Rahman, M. Saad , and P. Archambault, "Force-position control of a robotic exoskeleton to provide upper extremity movement assistance," International Journal of Modelling, Identification and Control, vol. 21, pp. 390-400, Jan 2014.

[71]   M. H. Rahman, T. O. Kittel, M. Saad, J. P. Kenné, and P. S. Archambault, "Development and control of a robotic exoskeleton for shoulder, elbow and forearm movement

assistance," Applied Bionics and Biomechanics, vol. 9, pp. 275-92, 2012.

[72] C. O. Luna, M.H. Rahman, M. Saad, P. Archambault, and W. H. Zhu, "Virtual decomposition control of an exoskeleton robot arm," Robotica, vol. 34(7), pp. 1587-609, Jul 2016.

[73] M. Rahmani, H. Komijani, A. Ghanbari, and M. M. Ettefagh, "Optimal novel super-twisting PID sliding mode control of a MEMS gyroscope based on multi-objective bat algorithm," Microsystem Technologies, vol. 24, pp. 2835-46, Jun 2018.

[74] M. Rahmani and M. H. Rahman, "Novel robust control of a 7-DOF exoskeleton robot" PloS one, vol. 13, pp. e0203440, Sep 2018.

[75] P. Kachroo and M. Tomizuka, "Integral action for chattering reduction and error convergence in sliding mode control," In1992 American Control Conference, pp. 867-870, Jun 1992.

[76] Tays, G., Bao, S., Javidialsaadi, M., & Wang, J. (2020). Consolidation of use-dependent motor memories induced by passive movement training. Neuroscience Letters, 135080.